EXPERIMENTAL INVESTIGATION ON IMPLEMENTATION OF THERMOELECTRIC MODULES IN A CONDENSER TUMBLE DRYER

by
Murat Orçun Kaplan

Submitted to Graduate School of Natural and Applied Sciences
in Partial Fulfillment of the Requirements
for the Degree of Master of Science in
Mechanical Engineering

Yeditepe University
2018

EXPERIMENTAL INVESTIGATION ON IMPLEMENTATION OF THERMOELECTRIC MODULES IN A CONDENSER TUMBLE DRYER

APPROVED BY:

Prof. Dr. Hojin Ahn   ....

(Thesis Supervisor)
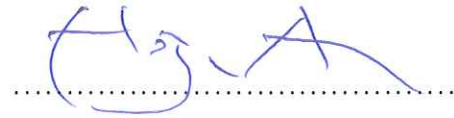
Assist. Prof. Dr. Ali Bahadır Olcay   ....

Assist. Prof. Dr. Barış Yılmaz   ....

DATE OF APPROVAL: …. /…. /2018

ACKNOWLEDGEMENTS

First of all, I would like to thank my thesis supervisor Prof. Dr. Hojin Ahn for his guidance and support during my thesis period.

I also acknowledge my wife and my family for giving great support to complete my thesis.

The Ministry of Science, Industry and Technology of Turkey (SAN-TEZ) is also acknowledged for financial support during my master education.

This study is accomplished with the extensive support of Arçelik A.Ş. So, I would like to thank Arçelik Research and Development Department and present my appreciation for my master education.

I especially acknowledge Yavuz Şahin and Onur Hartoka, engineers at Arçelik A.Ş., who always supported me not only during my thesis studies but also whenever I needed them.

Lastly, I would like to thank Bahadır Erol, Cansın Karadeniz and Enis Ürel for their lifetime friendship.

ABSTRACT

EXPERIMENTAL INVESTIGATION ON IMPLEMENTATION OF THERMOELECTRIC MODULES IN A CONDENSER TUMBLE DRYER

The objective of the project is to implement the use of thermoelectric modules in the condenser tumble dryer for the purpose of reduction in specific energy consumption. The thermoelectric technology is surveyed and parameters affecting the performance of thermoelectric modules are examined. Heat exchangers are designed for both hot and cold sides of the thermoelectric modules, and a heatsink testing setup is constructed in order to compare different heat exchanger performances. Finally, the condenser and thermoelectric modules are incorporated into a few prototypes, and the reduction of specific energy consumption is examined.

ÖZET

TERMOELEKTRİK SOĞUTMA SİSTEMLERİNİN KONDENSERLİ KURUTUCU MAKİNELERİNE UYGULANABİLİRLİĞİNİN DENEYSEL OLARAK İNCELENMESİ

Bu proje ile termoelektrik modüllerin yoğuşturuculu çamaşır kurutma makinesine uygulanarak enerji tüketimi değerinin azaltılması amaçlanmıştır. Bu kapsamda termoelektrik teknolojisi araştırılmış ve termoelektrik modüllerin performansını etkileyen parametreler incelenmiştir. Termoelektrik modüllerin hem sıcak hem soğuk tarafında kullanılmak üzere ısı değiştirici tasarımları yapılmıştır. Ayrıca ısı değiştiricisi deney düzeneği kurularak farklı ısı değiştiricilerin termal özelliklerinin ölçümü gerçekleştirilmiştir. Son olarak termoelektrik modüllerin ve yoğuşturucunun birleştirildiği melez çamaşır kurutma makinesi prototipleri ile erişilen enerji tüketimi değerleri incelenmiştir.

TABLE OF CONTENTS

LIST OF FIGURES

LIST OF TABLES

LIST OF SYMBOLS / ABBREVIATIONS

DT_{sys}	Temperature difference between the ambients that are cooled and heated
DT_{tec}	Temperature difference between the surfaces of thermoelectric module
E_{label}	Energy consumption that can be labelled
E_{total}	Total energy consumption during the drying operation
I	Operating current of thermoelectric module
I_{max}	Max operating current of thermoelectric module
$m_{laundry}$	Wet laundry mass
$m_{laundry,0}$	Dry laundry mass
Q_c	Heat absorbed from the system that is being cooled
$Q_{c,max}$	Max cooling power that can be absorbed from the cold surface
Q_h	Heat dissipated from the system that is being heated
R	Thermoelectric module electrical resistance
$R_{th,cs}$	Thermal resistance of the cold sink
$R_{th,hs}$	Thermal resistance of the heat sink
S	Seeback coefficient
T_{amb}	Temperature of the ambient that is being heated
T_{cold}	Temperature of cold surface of the thermoelectric module
T_{hot}	Temperature of hot surface of the thermoelectric module
T_{load}	Temperature of the ambient that is being cooled
UA_{hs}	Thermal conductivity of heatsink
UA_{cs}	Thermal conductivity of coldsink
V	Operating voltage of thermoelectric module
V_{max}	Max operating voltage of thermoelectric module
ΔT_{sys}	Temperature difference between the ambients that are cooled and heated
ΔT_{tec}	Temperature difference between the surfaces of thermoelectric module
ΔT_{max}	Max temperature difference between the surfaces of thermoelectric module
μ_i	Initial actual moisture mass percentage in a laundry
μ_f	Final actual moisture mass percentage in a laundry

Θ_{tec}	Thermal resistance of thermoelectric module
COP_{tec}	Coefficient of performance for thermoelectric module
CTS	Condenser test setup
REF*	Reference specific energy consumption of a condenser tumble dryer
SE	Specific energy consumption
TEC	Thermoelectric cooler module

1. INTRODUCTION

1.1. BASICS OF THERMOELECTRIC COOLING

Thermoelectric coolers are consisting of semiconductors that are arranged in a special order which enables to transfer heat from one side of the module to another. The heat is moved in the direction of the current by applying a low voltage, high current, DC power source. This is also known as Peltier Effect. This effect is basically the opposite of Seebeck Effect which thermocouples are based on and was discovered by Charles Athanase Peltier in 1834. [1] Semiconductor technology had a breakthrough especially after 1950s and Peltier effect started to be used in various applications.

Thermoelectric cooling is provided by the DC current flow through the couples of N and P type semiconductors. The heat moves in the same direction with the electrons within the N type semiconductors while it moves in the direction of hole flow within the P type semiconductors. The configuration of the serially connected P-N multi-couples allows the enhancement of the heat-pumping capacity. [2] (Figure 1.1)
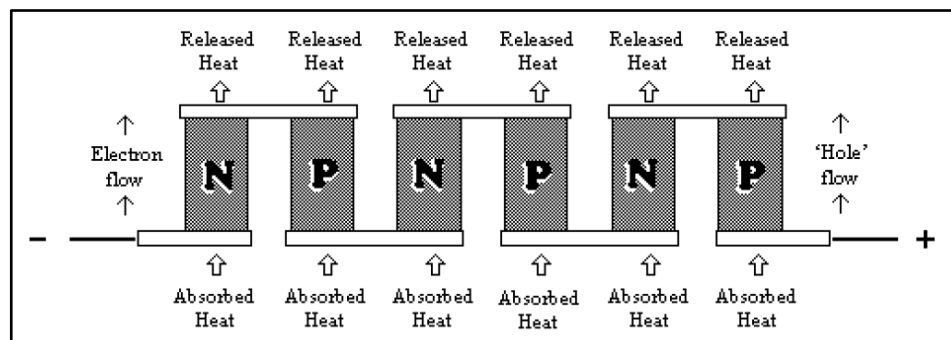
Figure 1.1. Multi-couple configuration increases heat-pumping capacity

P-N multi-couples are made of various semiconductor alloys such as Bi_2Te_3, PbTe, SiGe and BiSb. Bismuth Telluride is the most common material that is being used in commercial applications due to its high thermoelectric efficiency and appropriate working temperature range.

P-N multi-couples are connected to each other with the high thermal conductors such as copper or aluminum and placed in ceramic substrates in order to provide high electrical insulation, thermal conductivity and mechanical endurance (Figure 1.2). The performance of the module varies with the materials used. [3]
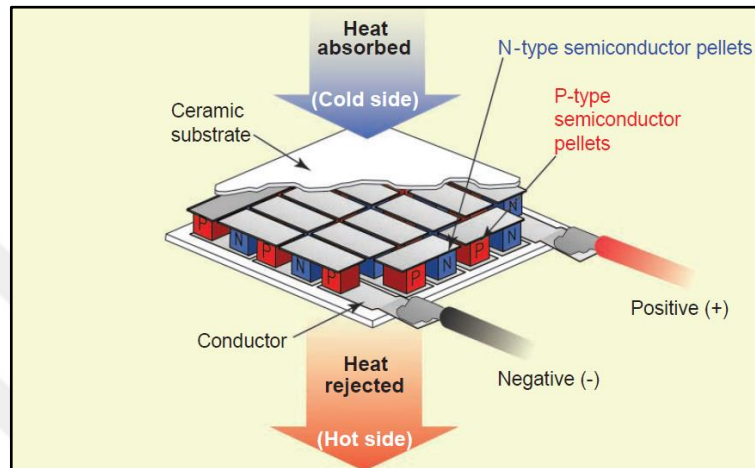
Figure 1.2. A thermoelectric module with the demonstration of P-N configuration

1.2. ADVANTAGES AND DISADVANTAGES

Thermoelectric coolers have the following advantages relative to the other cooling systems;

- They do not need much maintenance since they have no moving parts.
- They are quiet and solid products.
- They are ecologically friendly products since they do not include any refrigerants like the other compression type cooling systems.
- They are fully-reversible heat pumps. The heat flow can be easily reversed by only changing the direction of current flow.
- They are operational even in zero gravity environment without being affected by their standing position.
- They enable very accurate temperature control.

Thermoelectric coolers have the following disadvantages;

- They have low COP of heating and cooling.
- They require DC electric supply.
- They are currently expensive.

Considering the advantages and disadvantages of thermoelectric coolers, so far, they have achieved to take place in medicine and electronic sectors, refreshments and tertiary industries, scientific and military researches such as electronic circuit coolers, dress coolers, mobile coolers, etc. [4]

1.3.   SELECTION OF THERMOELECTRIC MODULE PARAMETERS
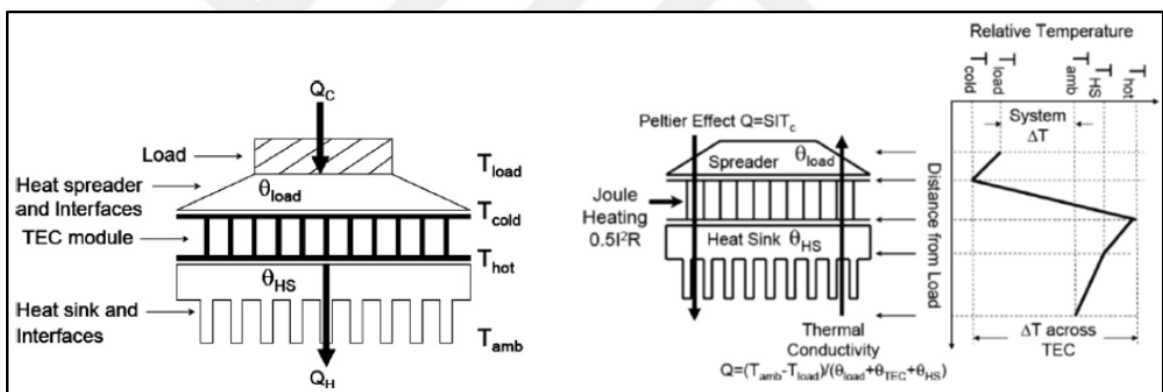
Figure 1.3. Thermoelectric cooling system

General thermoelectric cooling system is shown in Figure 1.3. In this system, thermoelectric module suppliers share ΔT_{max}, V_{max}, I_{max} and $Q_{c,max}$ parameters of their products as a specification. $Q_{c,max}$ is defined as the theoretical maximum cooling power that can be obtained when the temperature difference between the module surfaces is zero and ΔT_{max} is defined as the maximum temperature difference of the surfaces that can be obtained. Cooling process stops when ΔT_{max} is reached.
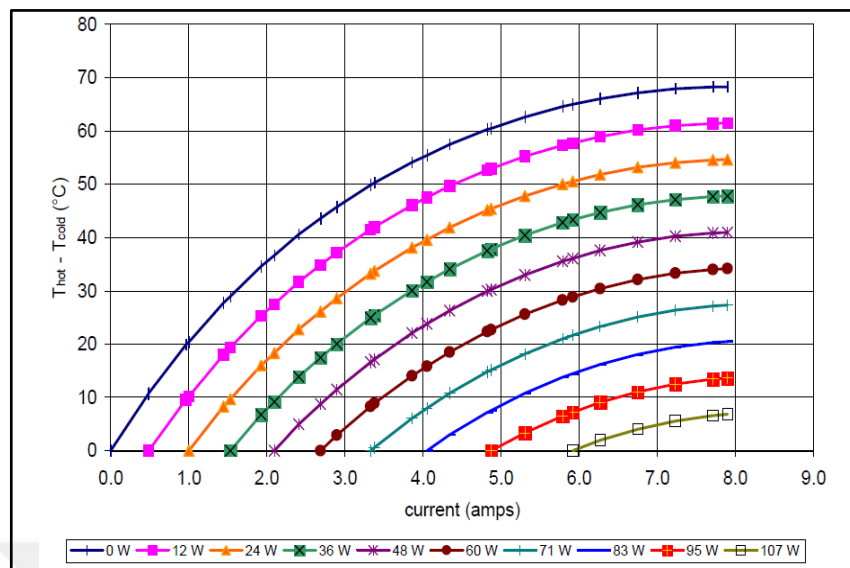
Figure 1.4. An example of thermoelectric module cooling power curve

As shown in Figure 1.4, the cooling power of the module decreases with the increasing temperature difference between its surfaces for a given feeding current. However, the cooling power increases with the increasing current for a constant temperature difference of the module surfaces. The cooling power reaches zero as the temperature difference goes to maximum. [5]
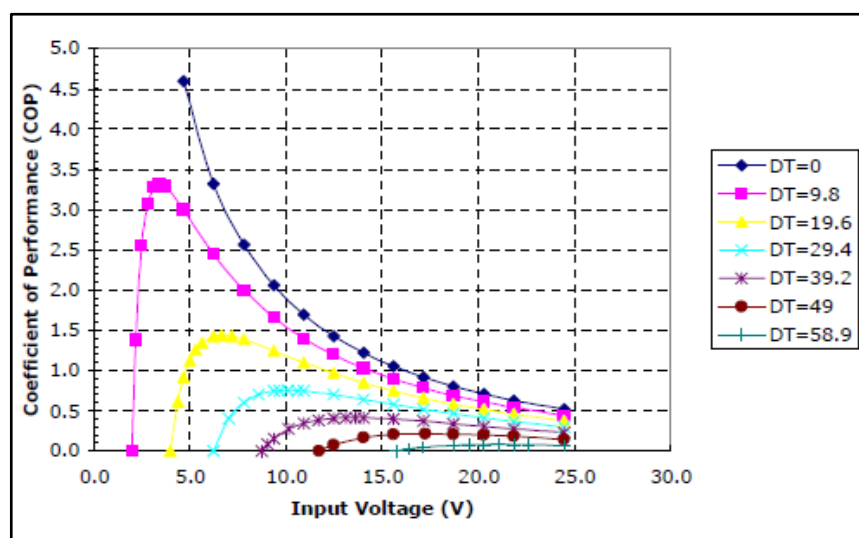
Figure 1.5. An example of thermoelectric module cooling efficiency based on temperature and feeding current

As for the heat pump efficiency of the thermoelectric cooler, the change of COP is shown in Figure 1.5. It is seen that COP value increases when the temperature difference (DT=ΔT) is reduced.

F.L. Tan and S.C. Fok have explained their study on obtaining the high thermoelectric module performance in the article that was published in 2006. [6] In this study they have used the parameters that are specified by the suppliers and they defined some formulas such as;

Thermoelectric module resistance:

$$R = \frac{V_{max}}{I_{max}} \frac{(T_{hot} - \Delta T_{max})}{T_{hot}} \qquad (1.1)$$

Seeback coefficient:

$$S = \frac{V_{max}}{T_{hot}} \qquad (1.2)$$

Thermal Power that is absorbed from the cold surface of the thermoelectric module:

$$Q_c = ST_{cold}I - \frac{1}{2}I^2 R - \frac{\Delta T}{\theta_{TEC}} \qquad (1.3)$$

Thermoelectric module voltage:

$$V = S\Delta T + IR \qquad (1.4)$$

Thermoelectric module power supply:

$$P = IV \qquad (1.5)$$

Heat dissipated from the hot surface:

$$Q_h = Q_c + P \qquad (1.6)$$

Coefficient of Performance (Cooling Efficiency):

$$COP = \frac{Q_c}{P} \tag{1.7}$$

In this project, a calculation tool has been created by Prof. Dr. Hojin Ahn with the help of these formulas and the paper by S. B. Riffat and X. Ma in order to derive the performance curves of any thermoelectric module of which ΔT_{max}, V_{max}, I_{max} and $Q_{c,max}$ parameters are given. [7]

HARDWARE SPECIFICATION

Imax	7,9	ampere
Vmax	24,6	volt
dTmax	69	K
T_hot	300	K
R=	2,397722	ohm	electrical resistance
S=	0,082	V/K	TEC Seebeck coeffici
theta_TEC	0,922202	K/W	thermal resistance of

Performance calculation for the given hardware

T_hot	373	K
Qc	40	W
dT	40	K
a=	1,198861	
b=	-27,306	
c=	83,37443	
I=	3,632738	A
V=	11,99029	V
P=	43,5576	W
COP=	0,918324	
Qh	83,5576	W

Optimum performance calculation for the given hardware

Tc	333
dT	40
I_opt=	3,570953
V_opt=	11,84215
P_opt=	42,28776
Qc=	38,84649
COP_opt=	0,918622
Qh	81,13425

TEC (thermalelectronic cooler)

HARDWARE SPECIFICATION

Imax	7,9	ampere
Vmax	24,6	volt
dTmax	69	K
T_hot	300	K
R=	2,397722	ohm
S=	0,082	V/K
theta_TEC	0,922202	K/W

V	12,5	31,8
I	2,97	
DT	26,11	
Tcold	328,31	55,31
Thot	354,42	81,42
Qc	41,06892	
COP	1,106234	
Qh	78,19392	703,7453

Figure 1.6. A view of TEC calculation tool
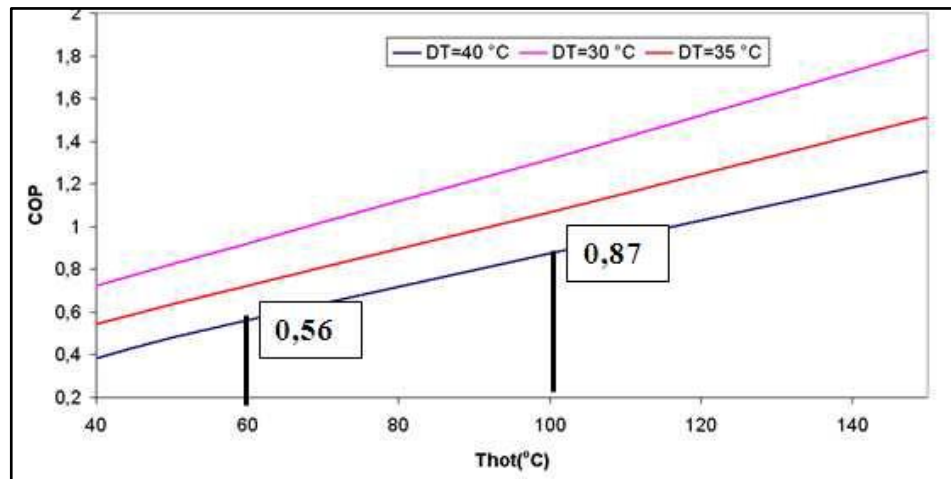
Figure 1.7. TEC module efficiency (COP) versus the hot surface temperature (T_{hot}) for various DTs

Figure 1.7 shows that thermoelectric module COP value increases as T_{hot} value increases for a given temperature difference.
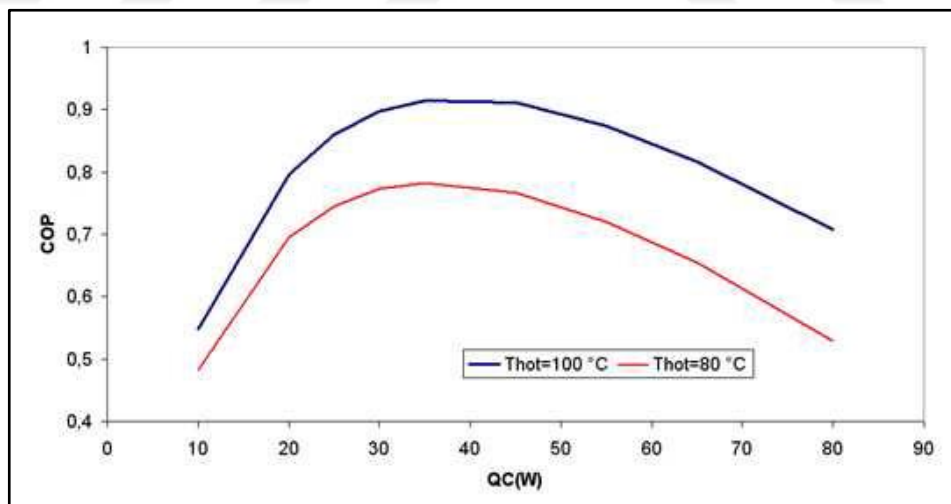
Figure 1.8. TEC module efficiency (COP) as a function of cooling power (Qc) for various hot surface temperatures

Figure 1.8 presents COP as a function of the cooling power (Q_c). As the cooling power changes, there is a maximum COP region. It is also noted that the higher hot surface temperature (T_{hot}), the higher COP. [8]

2. DESIGN OF THE HYBRID TUMBLE DRYER

2.1. CONVENTIONAL TUMBLE DRYERS

The most conventional type of tumble dryers is air vented dryers which have an open cycle process. Low temperature air is entered from the ambient by the help of a fan and heated by an electrical heater. The hot air passes through the clothes in the tumble, allows the liquid water on the textiles to evaporate. Then the humid air leaves the drum, passes through the lint filter, and then is evacuated outside. This type of tumble dryers is not desirable due to the fact that the humid air needs to be thrown out to the environment.

In air condenser type dryers, there are one cooling cycle and one closed cycle process. The air in the closed cycle process is heated by the help of an electrical heater in order to decrease its relative humidity, and enters into the tumble. The hot and dry air evaporates the moisture from the clothes and its humidity increases. After that humid air passes through the lint filter and fan, and then the condenser. The condenser cools down the process air and thus moisture in the air is condensed by the help of ambient air which is provided by another fan in the cooling cycle. The condensed water is discharged to a tank or drainage. This type of dryers has become more preferable as they are more energy efficient compared to air vented dryers.

The most energy efficient type of tumble dryers are heat pump dryers. Unlike air condenser dryers, they have an evaporator in addition to the condenser instead of heater in the process cycle. In the cooling cycle, the compressor with the help of refrigerant enables to eliminate the heater in the main process and makes the heat recovered from the evaporator in order to be used to increase the process air temperature in the condenser. Due to high manufacturing costs, the heat pump dryers are more expensive, and this is the reason for not being preferred even if they have much lower energy consumption levels in the market. [9]

2.2. EUROPEAN EFFICIENCY REQUIREMENTS

The BS EN 61121:2005 standard defines the classification of energy consumption levels and methods for measuring performance for tumble dryers sold in Europe. According to the European energy labeling system (Table2.1), there is no conventional air vented or condenser type tumble dryer that has achieved A class label in the market.

According to the EN 61121:2005, the total energy consumption of a tumble dryer (E_{Label}) that can be declared by the manufacturer on the product label is calculated by testing a specifically defined cotton laundry that is wetted with water under defined conditions. The declared energy consumption of the laundry depends on the measured energy consumption, the ratio of the nominal moisture content to the actual moisture content and also the ratio of the rated capacity of the program to the conditioned mass of the laundry. The measured value of energy consumption shall not be greater than the declared value by more than 6 per cent. [10]

$$E_{Label} = E_{Total} \cdot \frac{1.14(\mu_{i0} - \mu_{f0})m_{laundry}}{(\mu_i - \mu_f)m_{laundry_0}} \tag{2.1}$$

The nominal moisture contents of the laundry are 60 percent at the initial condition (μ_{f0}) and zero per cent at the final (μ_{i0}) condition.

Table 2.1. EU energy labels according to EN 61121:2005

EU Energy Label	Condensing Dryer Energy Consumption (kWh/kg)	Air-Vented Dryer Energy Consumption (kWh/kg)
A	EC <= 0.55	EC <=0.51
B	0.55 < EC <=0.64	0.51< EC <=0.59
C	0.64< EC <=0.73	0.59< EC <=0.67
D	0.73< EC <=0.82	0.67< EC <=0.75
E	0.82< EC <=0.91	0.75< EC <=0.83
F	0.91< EC <=1.00	0.83< EC <=0.91

2.3. HYBRID SYSTEM DESIGN FEASIBILITY
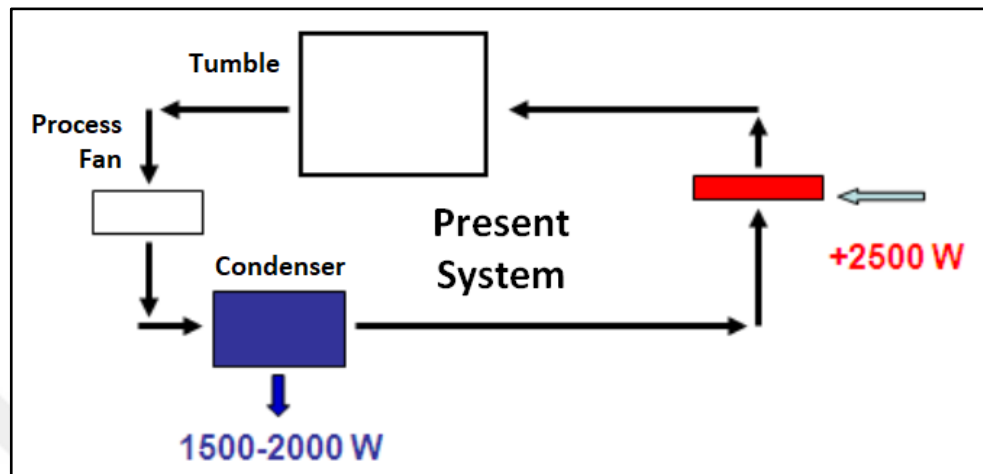
Figure 2.1. Air-cooled condenser dryer

Cooling and heating power requirements for a typical air-cooled condenser dryer are shown in Figure 2.1. A heater increases the temperature of the process air with the power of 2500W. A condenser cools the process air at the rate of 1500-2000W. The total energy consumption is shared by electrical heater and electric motor. The parameters which affects the energy consumption of the dryer are;

- Condenser efficiency
- Thermal loss
- Air leak
- Electric motor efficiency

Current condenser dryer energy consumption is used as reference (REF) in this study. Most of this energy is used to heat the laundries and vaporize the water. This inevitable portion is the biggest challenge in the way of achieving A class energy consumption in a dryer.
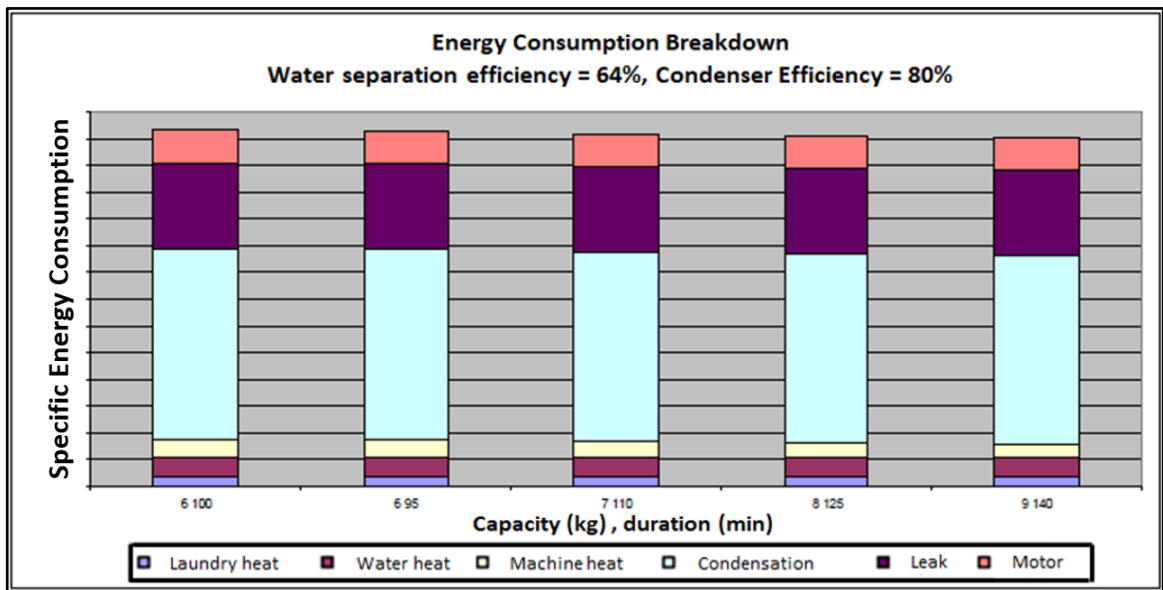
Figure 2.2. Condenser dryer energy consumption breakdown

Therefore, the aim of this study is to apply thermoelectric coolers which help energy recovery in order to reduce energy consumption of a condenser dryer. Unlike other known heat pump systems, thermoelectric modules are not able to provide all required heating and cooling capacity due to lower COP values with respect to the cooling cycles with compressors. A draft design of hybrid system using thermoelectric modules can be seen in Figure 2.3.
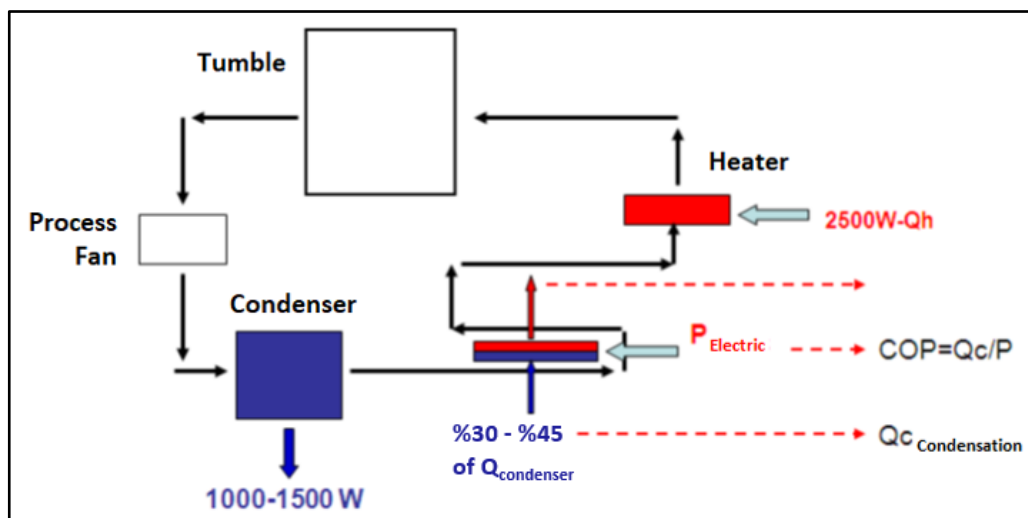
Figure 2.3. Hybrid system design

In this system, condenser and electric heater capacities are reduced and the deficient cooling and heating powers are supplemented by the cold and hot surfaces of the thermoelectric system. Additional cooling load of 30 per cent to 45 per cent of the condenser cooling load is provided by the cold surface of thermoelectric system. Similarly, the heating power of the electric heater is reduced by the amount of heating load provided by the hot surface of the thermoelectric system. The absorbed cooling load from the cold surface of thermoelectric system is directed to the hot surface of the thermoelectric system as energy recovery. In this way, total energy consumption is reduced based on the cooling load absorbed from the cold surface of the thermoelectric system.

In order to achieve an A class dryer, essential reduction of ultimate system energy consumption is calculated as 11 per cent compared to current condenser tumble dryers. Considering the expected energy loss based on thermoelectric module DC power supply circuit, the target system energy consumption is determined as 84 per cent of REF which requires 16 per cent of energy recovery with the help of hybrid system.
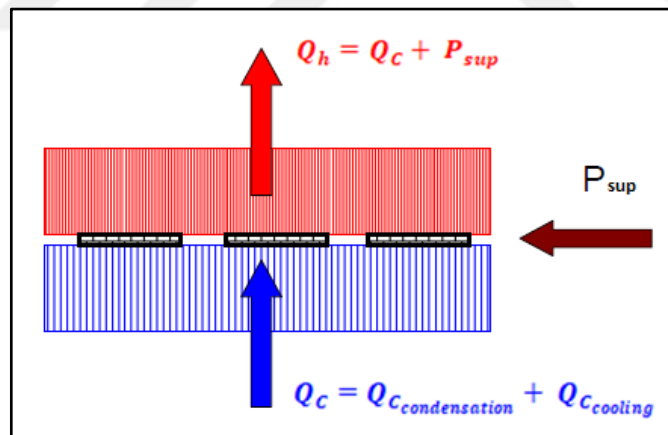
Figure 2.4. Hybrid tumble dryer thermoelectric energy equilibrium

As shown in Figure 2.4, the total heating power of the thermoelectric system is equal to the sum of condensation power, cooling power and electric power supplied to the system. Cooling power in cold surface of thermoelectric system is not a recovery due to the reheating power consumption in the hot surface unless the cooling load is used for condensation. The net heat recovery is obtained only by heat released in the condensation process at the cold surface of thermoelectric system. In this study, increasing the amount

and rate of condensation on the cold surface of the thermoelectric system is determined as one of the key parameters to reduce total energy consumption. The specific energy consumption of the hybrid system is calculated as shown below, based on the actual specific energy consumption of the condenser dryer and the required heating power assuming that the COP of the thermoelectric system remains constant.

$$SE_{Hybrid} = SE_{Cond}.\left(\frac{(Q_{tot}-Q_h)+\left(Q_h/_{\{(COP_c+1)\,\eta\}}\right)+P_{motor}}{Q_{tot}+P_{motor}}\right) \qquad (2.2)$$

With the help of above formula, the specific energy consumption of a hybrid system is calculated for different heating power variants and electrical efficiencies.
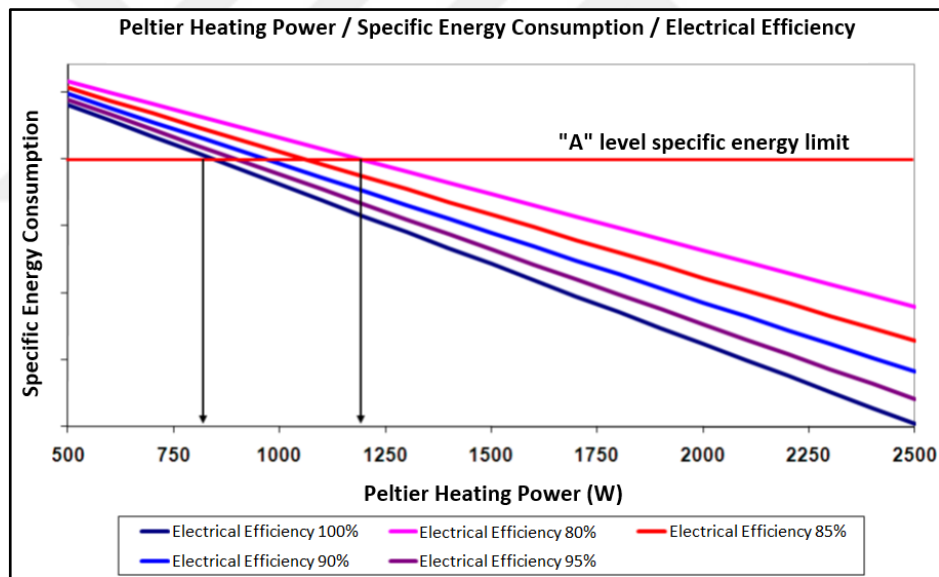
Figure 2.5. Thermoelectric module heating power & specific energy & electrical efficiency (COP=0.85)

The draft design parameters of the thermoelectric system are defined as shown in Figure 2.6. For a tumble dryer with the steady-state system temperature of 70°C, the cooling load of 450 W and the cold side exit temperature at 69°C, the heating power of 1000 W and the hot side exit temperature at 90°C are determined. As a result, thermoelectric module temperature difference is estimated as 40°C in these conditions.
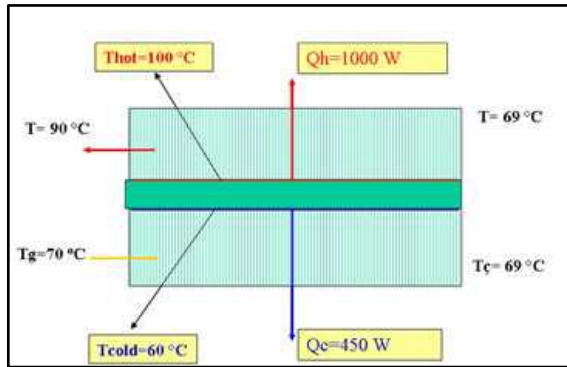
Figure 2.6. Draft design parameters of thermoelectric system

With these values, hot and cold side thermal resistance and conductivity constants are determined as follows;

- Hot side thermal resistance (R_{th}) & thermal conductivity (UA):

$$^1/_{UA} = R_{th} = (T_{hot} - T_{ave})/Q_h \cong \mathbf{0.02\ K/W,\ UA \cong 50\ W/K} \qquad (2.3)$$

- Cold side thermal resistance (R_{tc}) & thermal conductivity (UA):

$$^1/_{UA} = R_{tc} = (T_{hot} - T_{ave})/Q_c \cong \mathbf{0.022\ K/W,\ UA \cong 45\ W/K} \qquad (2.4)$$

2.4. HYBRID SYSTEM AIR FLOW CONFIGURATIONS

Five different air flow configurations are considered for the thermoelectric system in this study.

- Parallel air flow geometry
- S-shaped serial air flow geometry with two layers
- S-shaped serial air flow geometry with three layers
- S-shaped air flow geometry with three layers and by-pass
- S-shaped air flow geometry with four layers

2.4.1. Parallel Air Flow Geometry

The process air flows through the hot and cold side of thermoelectric module at the same time in this configuration as shown in Figure 2.7. The pressure drop would be reduced in this way but air flow rate is required to be carefully optimized in both hot and cold sides. All process air mass is not heated in the hot side of thermoelectric module. This configuration is patented by BSH.
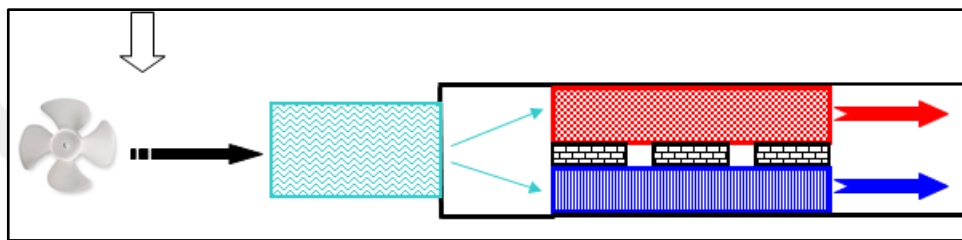
Figure 2.7. Parallel air flow geometry of thermoelectric system

2.4.2. S-shaped Serial Air Flow Geometry with Two Layers

The process air flows through the cold side of thermoelectric module and condenser at first and then the hot side of thermoelectric module in this configuration. The pressure drop would be high and the condenser cannot be removed in this configuration. Also, laundry lint in the process air holds on the heat exchangers of thermoelectric module. The right of this configuration belongs to AKG, a utility model in Germany.
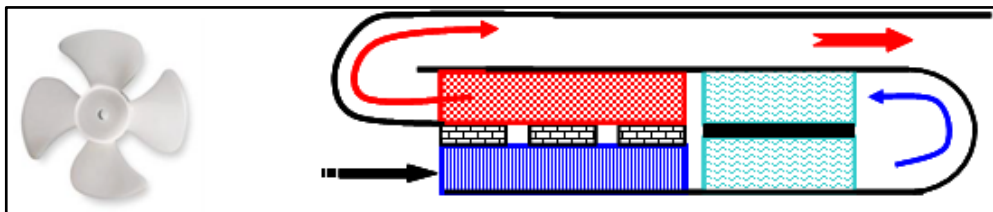
Figure 2.8. S-shaped serial air flow geometry with two layers

2.4.3. S-shaped Serial Air Flow Geometry with Three Layers

The humid process air flows through the air-cooled condenser in the first place to be cooled and condensed. After the condenser, air flows through the cold side of the thermoelectric module where additional condensation takes place. Finally, the process air flows through the hot side of the thermoelectric module, is heated and directed to the electrical heater before the tumble. The pressure drop is higher in this configuration because all air mass passes through all components in the system. Moreover, extra pressure drop occurs due to the S-shape of the channels. This configuration has been patented by Arçelik A.Ş.
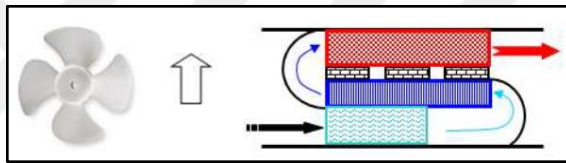
Figure 2.9. S-shaped serial air flow geometry with three layers

2.4.4. S-shaped Air Flow Geometry with Three Layers and a By-pass

Another configuration has been considered which has a by-pass channel between the outlet of cold side and inlet of hot side of thermoelectric module which allows some of the process air to pass through the hot side of thermoelectric module directly before going to the condenser. In this way, pressure drop based on S-channels is reduced. Furthermore, the condensation efficiency is expected to be improved by reducing air flow rate through the condenser and cold side of the thermoelectric module. This configuration has also been patented by Arçelik A.Ş.
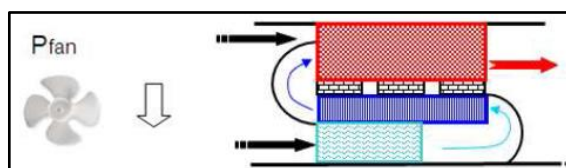
Figure 2.10. S-shaped air flow geometry with three layers and a by-pass

2.4.5. S-shaped Air Flow Geometry with Four Layers

In this configuration, a condenser and cold side of thermoelectric module are placed in parallel. The process air flows through the condenser and cold side of thermoelectric module at the same time so that the system pressure drop is reduced with respect to the serial configuration. The main disadvantages of this configuration are that lint would accumulate in the cold side of thermoelectric module and that it requires more space for the additional layer of the channel in the machine. Another disadvantage of this configuration is that the thermoelectric system COP would be lower due to the reduced condensation in the cold side of thermoelectric module.
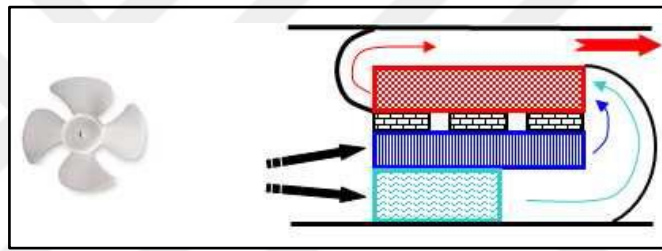
Figure 2.11. S-shaped air flow geometry with four layers

2.5. INITIAL EXPERIMENTS ON CONDENSER TEST SETUP

The Condenser Test Setup (CTS) is a test setup which was produced by Arçelik R&D engineers to develop more efficient condensers for tumble dryers. This test setup is modified in order to measure the performance of the initial thermoelectric system design under tumble dryer conditions.

As shown in Figure 2.12, CTS employs two radial fans by which flow rates can be adjusted as desired. One fan provides the cooling air flow through the condenser in the open cycle and the other fan controls the process air flow in the closed cycle. There are also an electrical heater and a humidifier in the closed cycle to keep the process air at the desired temperature and relative humidity. The draft thermoelectric system is placed downstream of the condenser in the process air path.
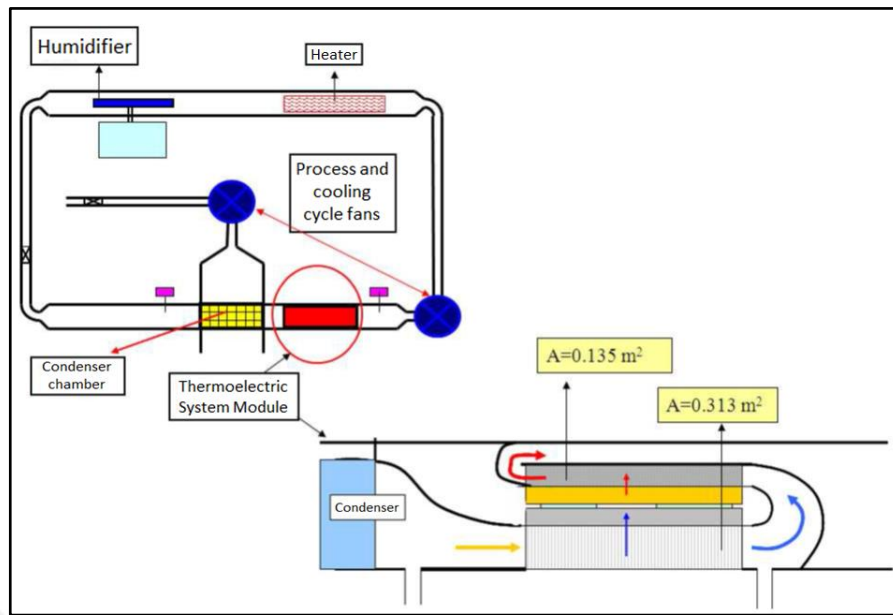
Figure 2.12. Thermoelectric system module in Condenser Test Setup

The draft thermoelectric system uses nine different thermoelectric modules (Peltier modules). As shown in Figure 2.13, the Peltier modules are connected to each other in three groups in order to power them with different DC suppliers. Thermodynamic and electrical data for each group are collected separately and the performance variations of three groups of thermoelectric modules are separately.
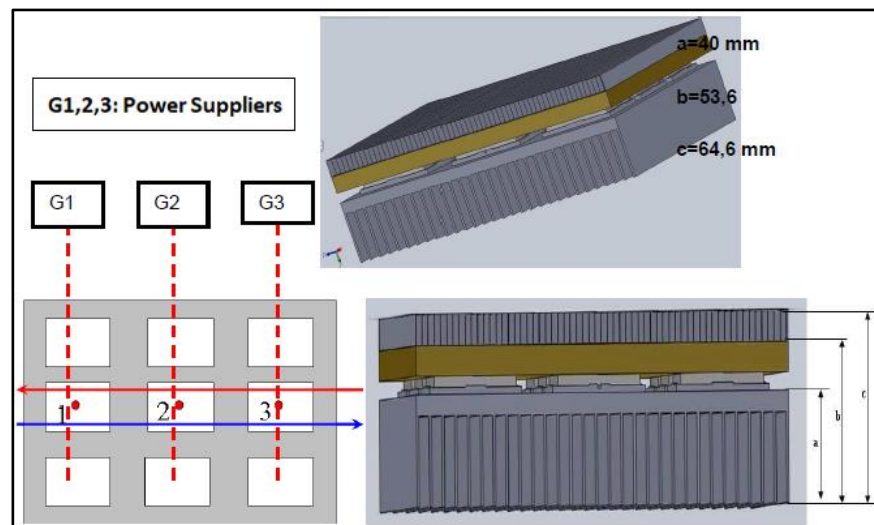
Figure 2.13. Thermoelectric module system design for CTS

Tetech branded HP-199-1.4-1.15 type of thermoelectric modules are selected for the initial prototype. The properties and COP of these modules for specific Q_c and Q_h values are shown in Figure 2.14. A heat exchanger with straight fins made from an aluminum block is used for the cold side of thermoelectric system. Another heat exchanger with complex fin design which is cut out of a condenser is used for the hot side of the initial thermoelectric system prototype. A copper block is also used for the heat dissipation between the thermoelectric modules and hot side heat exchanger. (Figure 2.15)

Brand	Model	Qmax	Imax	Vmax	DTmax
Tetech	H199-1.4-1.15	120	7,9	24,6	69
Tetech	H199-1.4-1.15-71	80	8	16,1	69
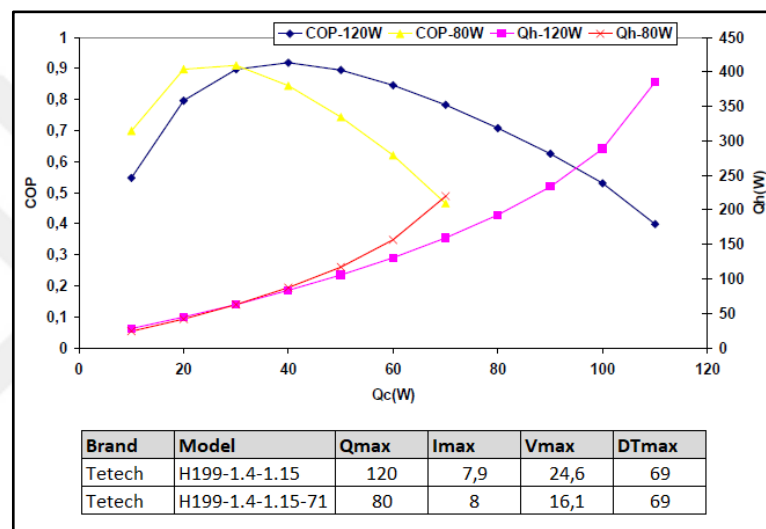
Figure 2.14. Theoretical performance values for the selected thermoelectric modules

Figure 2.15. Thermoelectric system prototype for CTS

During the tests at CTS, flow rates for process air and cooling air are fixed as 30 and 50 l/s, respectively. The inlet temperature and humidity of process air upstream of the condenser and the thermoelectric module are set to be at 70°C 90 per cent, respectively. The air temperatures in the inlet and outlet of cold side of thermoelectric system are measured as shown in Figure 2.16.
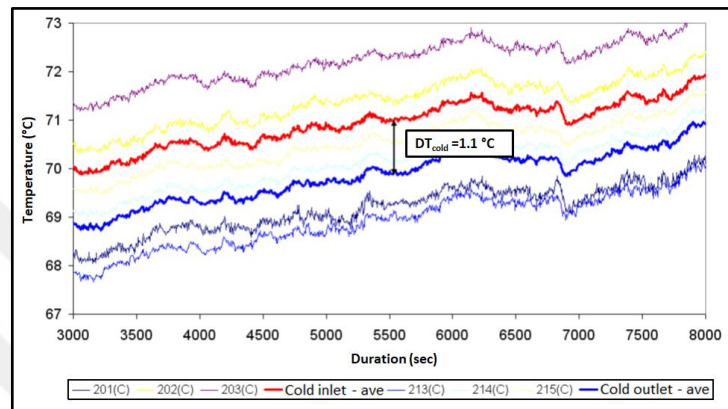
Figure 2.16. Air temperatures at the inlet & outlet of thermoelectric system

Figure 2.16 shows that the inlet temperature is approximately 71°C and the outlet temperature is approximately 69.9°C in the thermoelectric system. The average temperature difference between the inlet and outlet is determined as 1.1°C. The reason for this low temperature difference is the phase change of the water vapor in the air passing through the cold surface with high relative humidity.
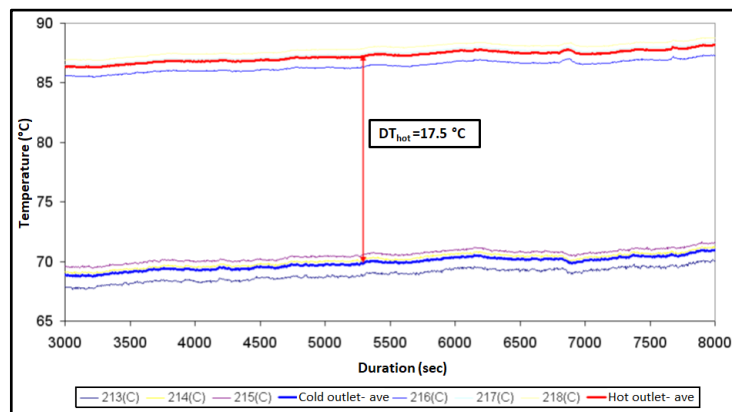
Figure 2.17. Cold side outlet and hot side outlet temperatures of thermoelectric system

On the other hand, Figure 2.17 shows that the hot side inlet and outlet temperature difference which is determined as 17.5°C in average.
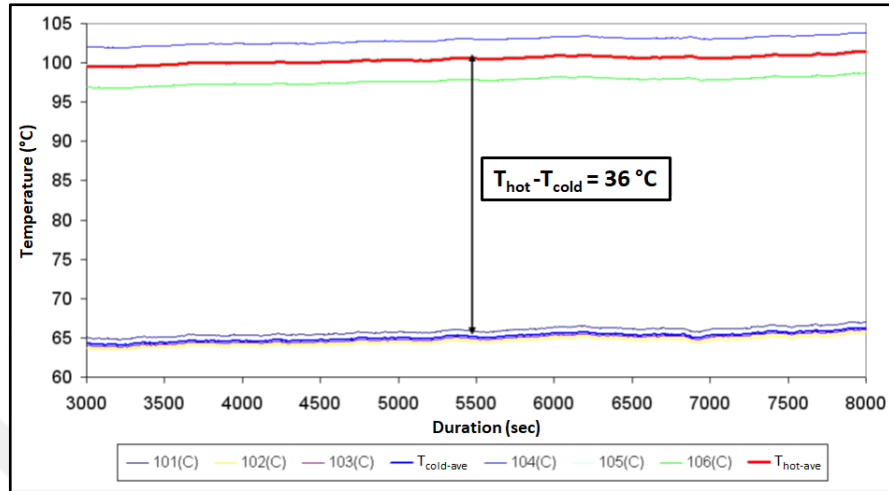
Figure 2.18. Average temperature difference of thermoelectric module surfaces

The average temperature difference between the hot and cold surfaces of the thermoelectric module is known as the most affecting parameter of thermoelectric module efficiency, and is measured to be 36°C as shown in Figure 2.18.
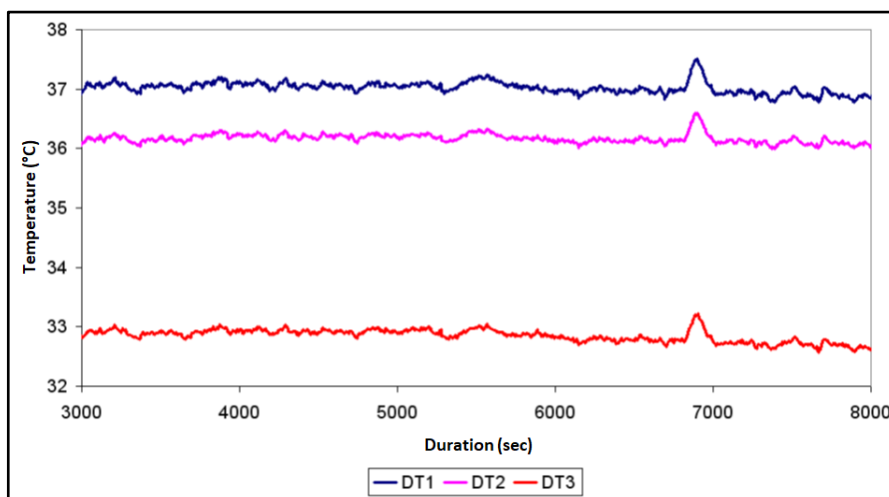
Figure 2.19. Thermoelectric module surface temperature differences for each group

The surface temperature differences for three groups of the thermoelectric modules are shown in Figure 2.19, and average temperature differences are 37°C for the first group, 36.2°C for the second group and 33°C for the third group.

Table 2.2. Thermoelectric module performance results

	DT (°C)	DC Voltage (V)	DC Current (A)	COP
Group 1	37	36.4	2.63	0.77
Group 2	36.2	36.2	2.72	0.83
Group 3	33	36	2.71	0.945

All thermodynamical and electrical data collected from this CTS experiment are used as input for the thermoelectric calculation tool and COP values are shown in Table 2.2.
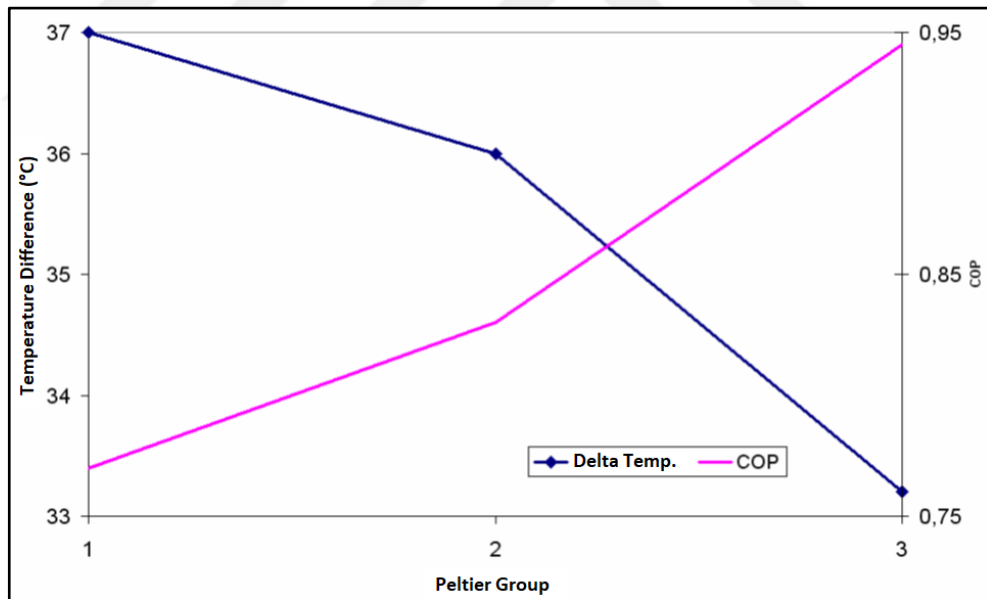
Figure 2.20. Temperature differences and COP values of thermoelectric module groups

As shown in Figure 2.20, COP value increases with the decreasing temperature difference of the thermoelectric module group.

Table 2.3. Cooling power, heating power and COP values of thermoelectric groups

	P (W)	Q_{cold} (W)	Q_{hot} (W)	COP
Group 1	95.7	74.1	169.8	0.774
Group 2	98.4	81.7	180.2	0.830
Group 3	97.6	92.2	189.7	0.945
Total	291.7	248	539.7	0.850

Table 2.3 shows the summary of the data obtained from the CTS experiment. It is noted that the heating and cooling capacities of each group of the thermoelectric module decrease in the direction of air flow in the hot side (3-2-1) (see Figure 2.13). The total cooling and heating powers are calculated to be 248 W and 539.7 W, respectively, while the input DC power is 291.7 W, and thus COP is calculated to be 0.850.

Table 2.4. Summary of initial CTS experiment results

	Temperature (°C)	Relative Humidity (%RH)	Specific Humidity (kg/kg)
Condenser Inlet	74.4	87.5	0.301
Peltier Cold Inlet	71.1	88.2	0.250
Peltier Cold Outlet	70.1	91.7	0.247
Peltier Hot Outlet	87.5	45	0.247
T_{cold} (°C)	65.3		
T_{hot} (°C)	100.6		
DT (K)	35.4		
Q_{hot} (W)	544.4		
Peltier Power (W)	291.7		
$Q_{hot\_theoretical}$ (W)	539.7		
$Q_{cold\_theoretical}$ (W)	248.0		
COP	0.850		

In the initial CTS experiment, the COP value of 0.85 is satisfactorily close to the COP target. However, the cooling power of 248 W is far from the cooling power target of 440W. The cooling power that can be obtained from the thermoelectric system depends on the temperature differences between the hot and cold surfaces of the thermoelectric module and on the performance of heat exchangers. It should be noted that the dimension of the thermoelectric module in the initial CTS experiment was smaller than the maximum allowable dimension in a dryer platform due to the condenser testing setup geometrical limitations. As a result, it is concluded that the target cooling power can be obtained by selecting appropriate heat exchangers (heatsink & coldsink) for the selected thermoelectric modules. Process air flow rate which is affected by pressure drop across the thermoelectric module system is also a significant parameter in addition to the heatsink selection.

3. HEAT EXCHANGER SELECTION

3.1. CFD ANALYSES

In the hybrid dryer project, a new heatsink design with different sizes and fin geometries is needed in order to obtain sufficient heat transfer on Peltier modules in different configuration and numbers. For this purpose, two different CFD analyses are conducted. In the first analysis, the peltier placement effect is examined with flat finned heatsink design under specified dimensions. The second analysis is conducted with a heatsink design with increased fin surface area under specified dimensions and 6 different peltier placement configurations.

3.1.1. CFD Analysis of Flat Finned Heatsink Design

The CFD model is constructed in Figure 3.1 in order to understand the effects of the Peltier module locations and distances among them on the outlet temperature. The boundary conditions are defined in this model as follows;

- Air temperatures at the heatsink inlet are specified from the experimental data. The heatsink inlet is divided into three regions with air flow at different temperatures of 342 K, 341.2 K and 340.9 K.
- Air flow rate is assumed to be uniform in the three regions.
- Analyses are conducted under a steady-state condition.
- The gaps between Peltier modules and heatsink walls are assumed to be adiabatic.
- The heating power of each Peltier module is assumed to be 80W.
- The channel heights are set to be 50mm at the inlet and outlet of the heatsink.

The mesh model has approximately three million hex elements and the realizable $\text{ƙ-}\varepsilon$ turbulence model is used for this analysis.
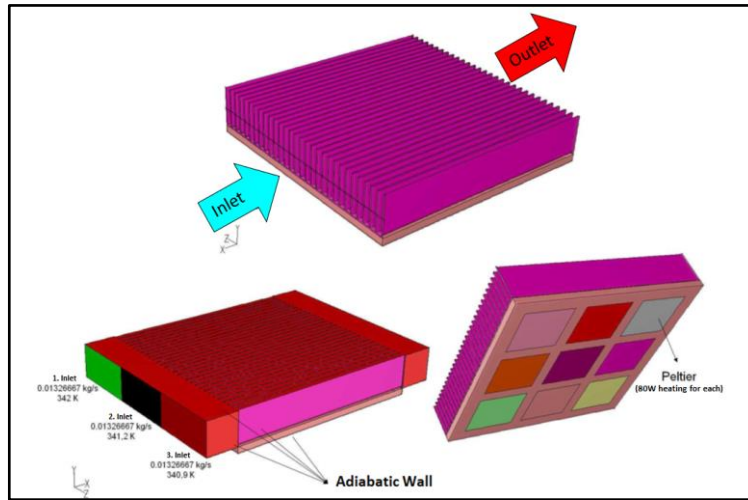
Figure 3.1. Heatsink model demonstration and boundary conditions

The first CFD analysis shows that temperatures vary on both fin surfaces and outlet air flow. Resultant temperature distributions on heatsink surface and inlet & outlet air flows are shown in Figures 3.2 and 3.3.
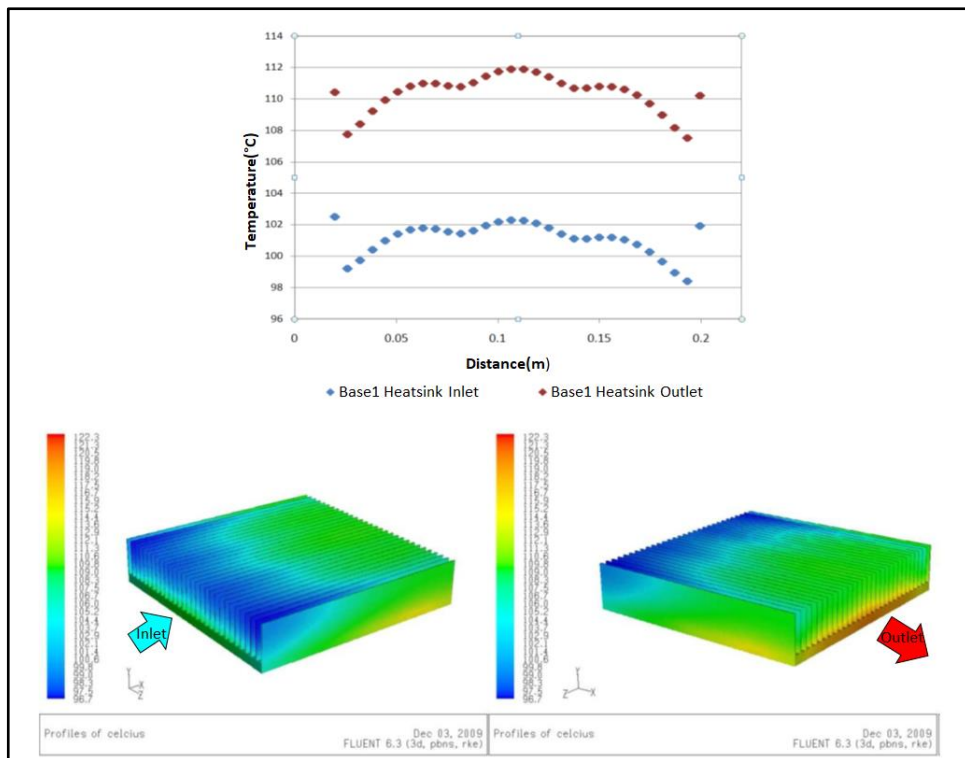
Figure 3.2. Temperature distribution for inlet & outlet air flow and heatsink surface
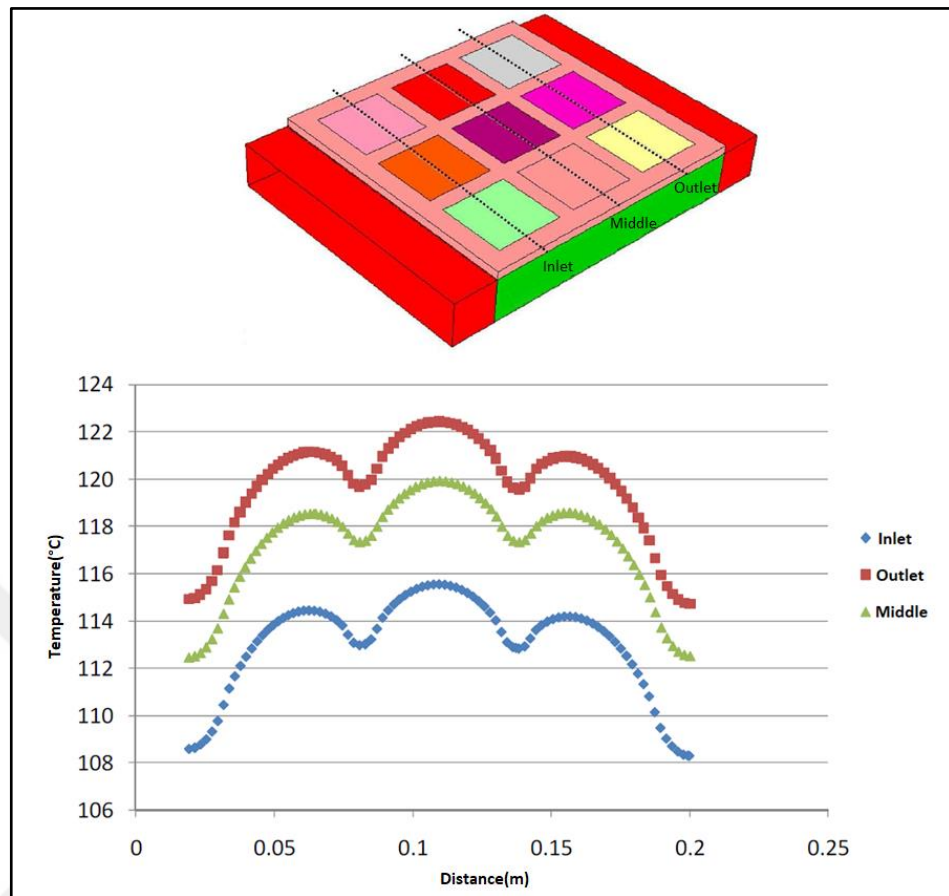
Figure 3.3. Peltier surface temperature distribution on the specified sections

3.1.2. CFD Analysis of Heatsink Design with Increased Fin Surface Area

Six different peltier module placement configurations are analyzed in this section in order to see the effect of different configurations on the performance of a heatsink which has fins with augmented surface area.

i.   250x250 mm – 9 Peltier modules
ii. 250x250 mm – 12 Peltier modules
iii. 250x200 mm – 9 Peltier modules
iv. 250x200 mm – 12 Peltier modules
v.   250x225 mm – 9 Peltier modules
vi. 250x225 mm – 12 Peltier modules
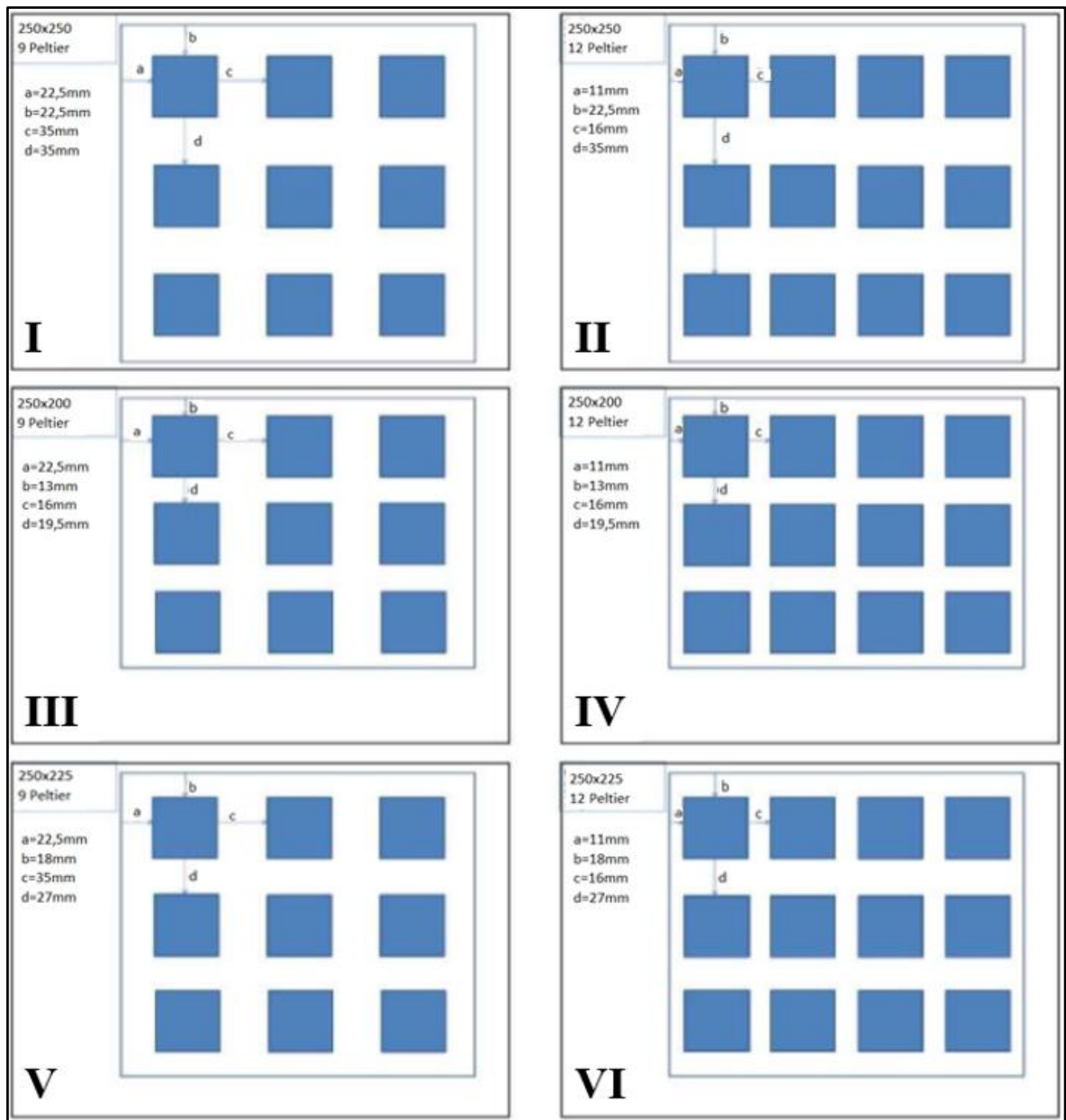
Figure 3.4. Six different Peltier replacement configurations

The boundary conditions are set in this model as follows;

- Air flow rate through the heatsink is 40 l/s and air temperature is 300K.
- Analyses are conducted under steady-state conditions.
- The gaps between Peltier modules and heatsink walls are assumed to be adiabatic.
- The total heating power of Peltier modules is set as 360W.
- The channel heights are 50 mm at the inlet and outlet of heatsink.

The mesh model includes approximately six million hex elements and the realizable ƙ-ɛ turbulence model is used for this analysis.
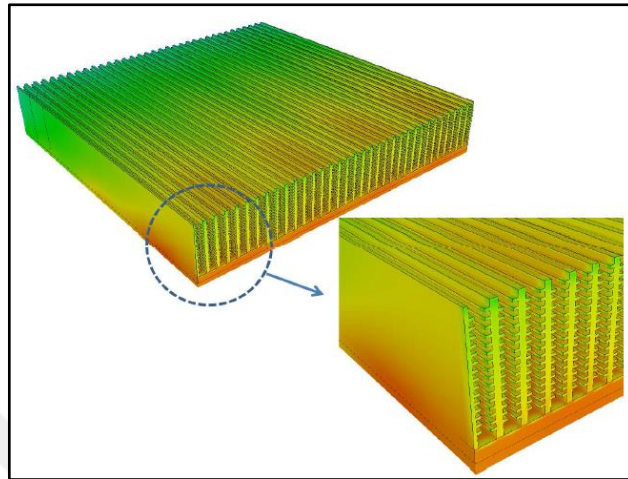
Figure 3.5. Detailed view of heatsink design with augmented fin surface area
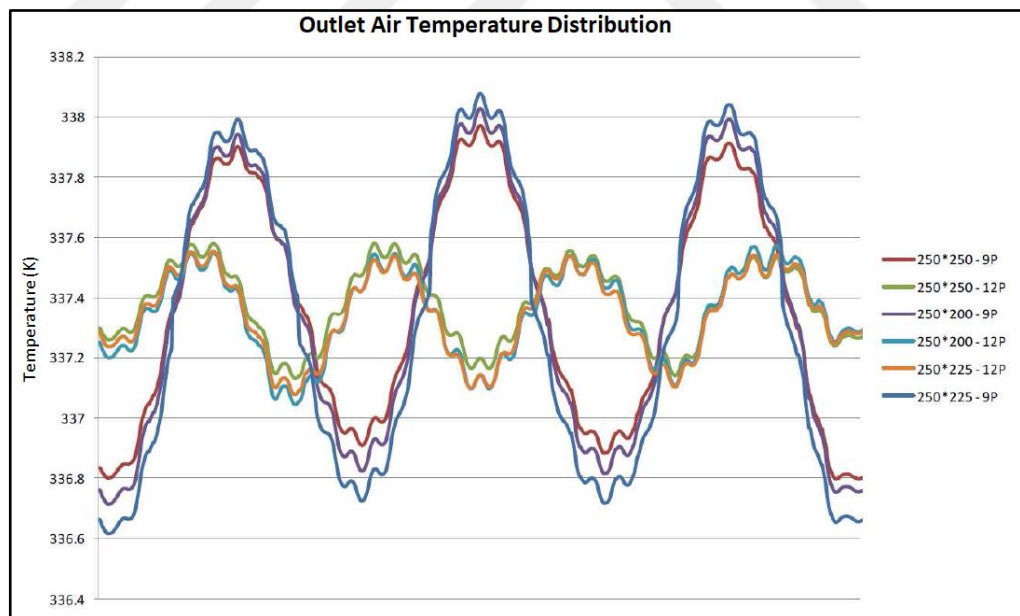
Figure 3.6. Heatsink outlet air temperature distributions for different configurations

The analyses results show that heatsink outlet air temperatures are changing with Peltier configurations and that the outlet air temperature is lower for the configurations with twelve Peltier modules.
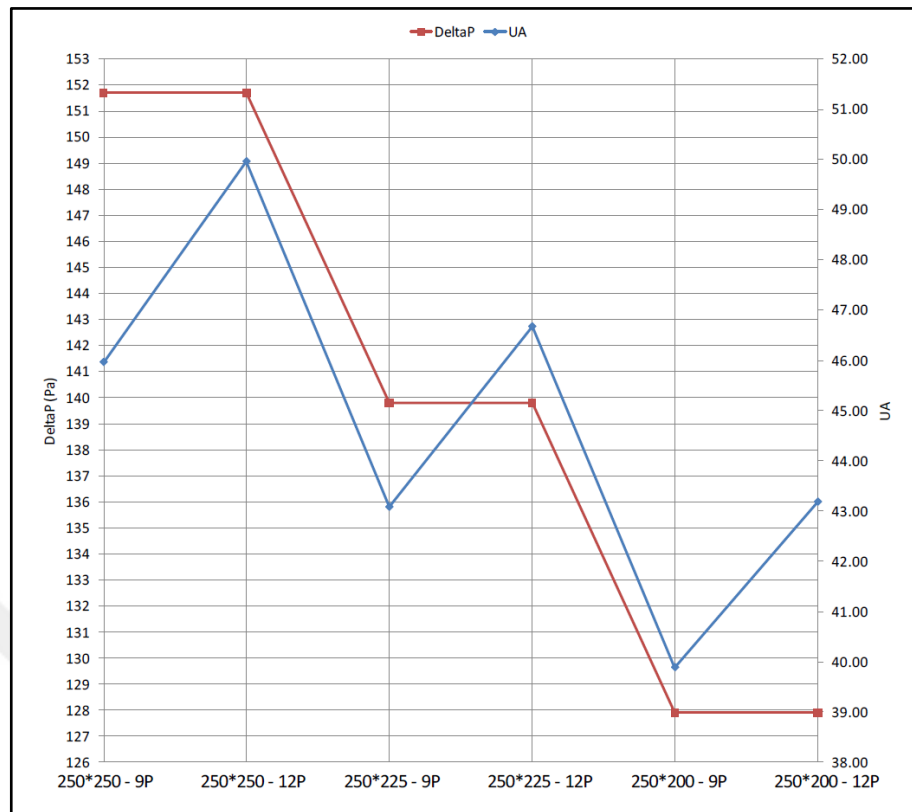
Figure 3.7. Pressure drop and thermal conductivity results based on heatsink length and Peltier number variation

Pressure drop and UA values are compared in Figure 3.7 for the six different configurations. The overall heat transfer coefficient is denoted as U [W/m^2] and the heatsink area is denoted as A [m^2]. The following observations have been made.

- UA value increases with the number of Peltier modules for the same heatsink length

- Both UA and pressure drop decrease with the smaller heatsink length.

- The UA value of 250x225-12P configuration is similar to that of 250x250-9P configuration although the pressure drop of 250x225-12P configuration is lower than that of 250x250-9P configuration.

In next sections, CFD results are supported with experimental data to improve heatsink performance further, and thus the thermoelectric system is optimized with lower pressure drop, higher UA value and the less number of Peltier modules.

3.2. HEATSINK TEST SETUP

In this project, it is decided to build a heatsink testing setup in order to determine the parameters affecting heatsink performance and examine the performances of different heatsink designs under various working conditions. Some articles which have been published for similar purposes are found in the literature search. [11]

As shown in Figure 3.8, the ambient air is driven through the heatsink in a wind tunnel by the help of a fan. Thermocouples and pressure probes are placed in the inlet and outlet of the heatsink in order to measure the temperature change and pressure drop. The fan is set for different air flow rates at which the heatsink pressure drop and thermal resistance values are calculated in the end.
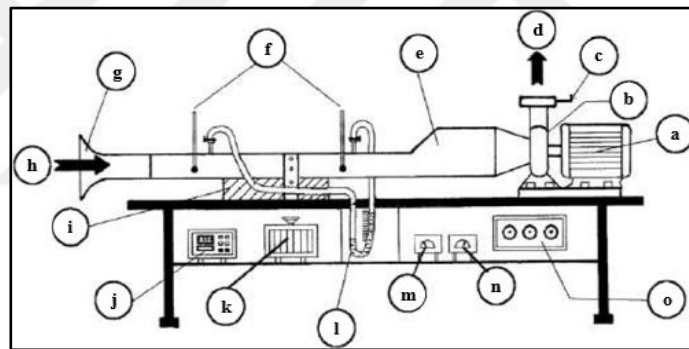
Figure 3.8. An example of a heatsink test setup. [11]
(a) Electric motor, (b) Suction air blower, (c) Air flow control gate, (d) Air outlet,
(e) Wooden duct, (f) Temperature probes, (g) Bell mouth, (h) Air inlet, (i) Test section,
(j) Digital temperature recorder, (k) Autotransformer, (l) Manometer, (m) Voltmeter,
(n) Ammeter, (o) Blower switchboard

Two plate type heaters are used to heat the heatsink as shown in Figure 3.9. A primary heater is placed under the heatsink and thermocouples are placed between the heater and heatsink to measure the bottom surface temperature of the heatsink. There is an insulator under the primary heater. The secondary heater is placed under the insulator and thermocouples are also located between the insulator and the secondary heater. The secondary heater is operated to equalize the temperatures above and below the insulator to ensure that all heating power of the primary heater is conducted to the heatsink.
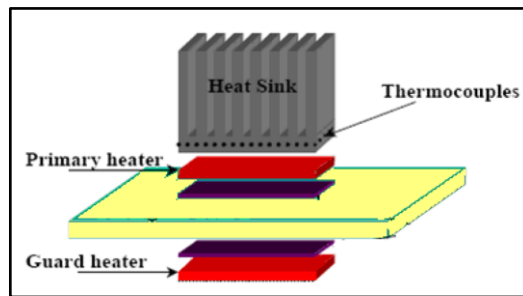
Figure 3.9. Heating setup of heatsink test setup

3.2.1. Heatsink Test Setup Design

As the first step of the test setup design process, the list of necessary components, their locations and their dimensions are determined.
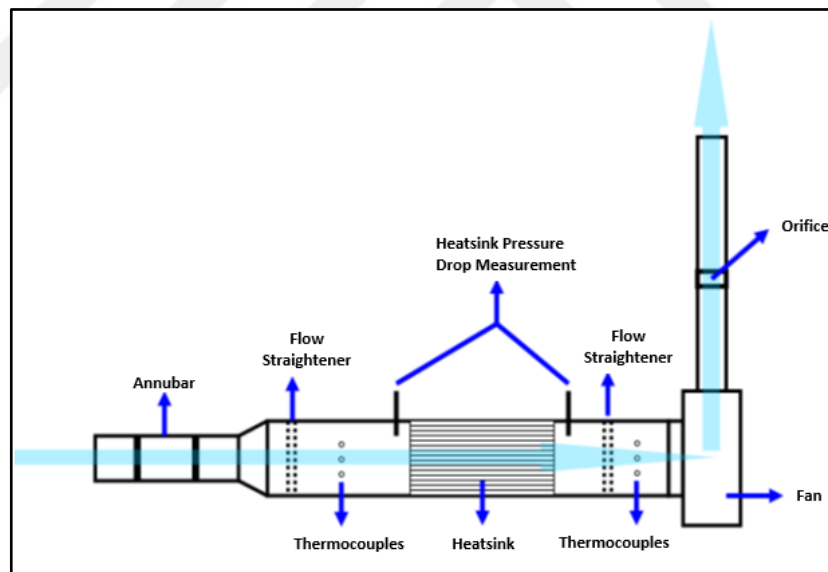
Figure 3.10. Top view of heatsink test setup

Both of an annubar in the entrance of the wind tunnel and an orifice in the exit of the wind tunnel provide redundant measurement of air flow rate. Flow straighteners are used in the inlet and outlet of the heatsink to make the air temperature uniform. Pressure probes and thermocouples are placed through the wind tunnel to measure air pressures and temperatures in the inlet and outlet of the heatsink.
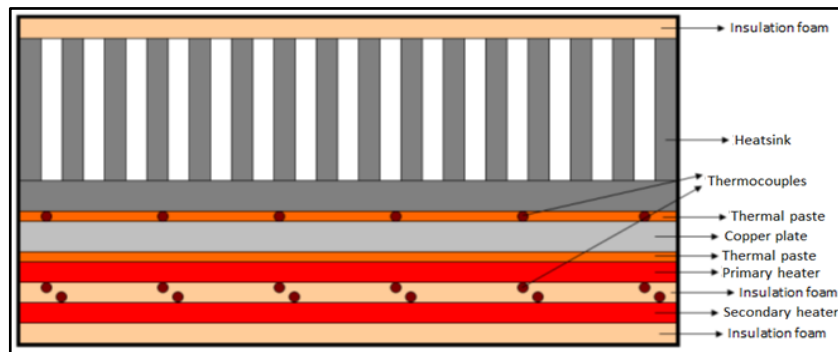
Figure 3.11. Heatsink and heaters placements

Heaters and heatsink placements are shown in Figure 3.11. A copper block, 15 mm in thickness, is used between the heatsink and the primary heater to provide uniform heat transfer from the heater to the heatsink bottom surface. Insulation foam and thermocouples are located below the primary heater, and the secondary heater power can be adjusted to equalize two temperatures below and above the insulation so that all primary heating power may be transferred to the heatsink.

The CAD model of heatsink test setup is presented in Figure 3.12. The dimensions of the tunnel are determined such that air may flow uniformly through the annubar, heatsink and orifice.
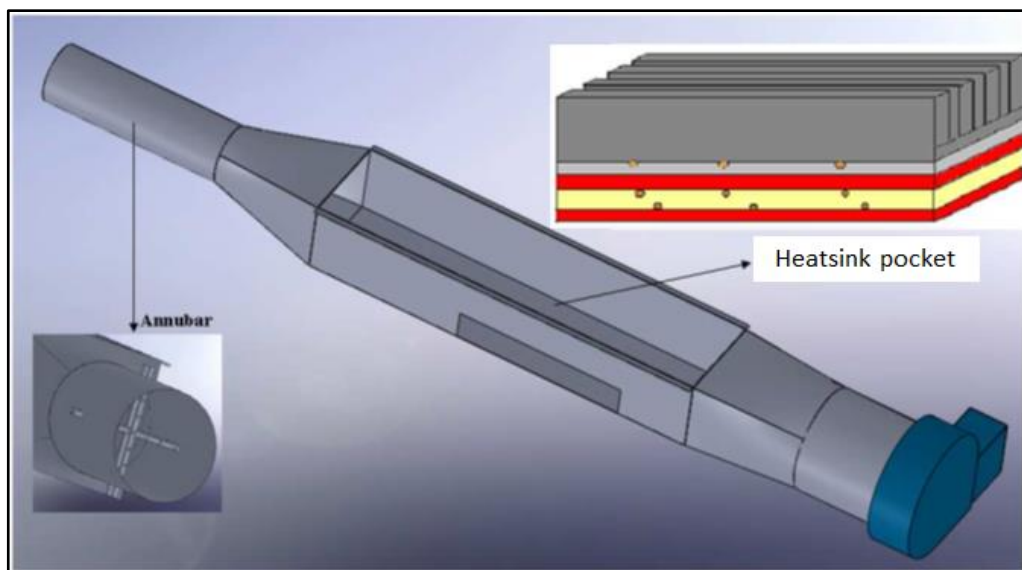
Figure 3.12. Heatsink Test Setup CAD model

An annubar system is designed, constructed and calibrated in a wind tunnel (Figure 3.13). Therefore, air flow rate is determined from the calibration curve after reading the output of the pressure sensor connected to the annubar.

Figure 3.13. Annubar system

The heatsink test setup is built by assembling all selected components as shown in Figure 3.14.
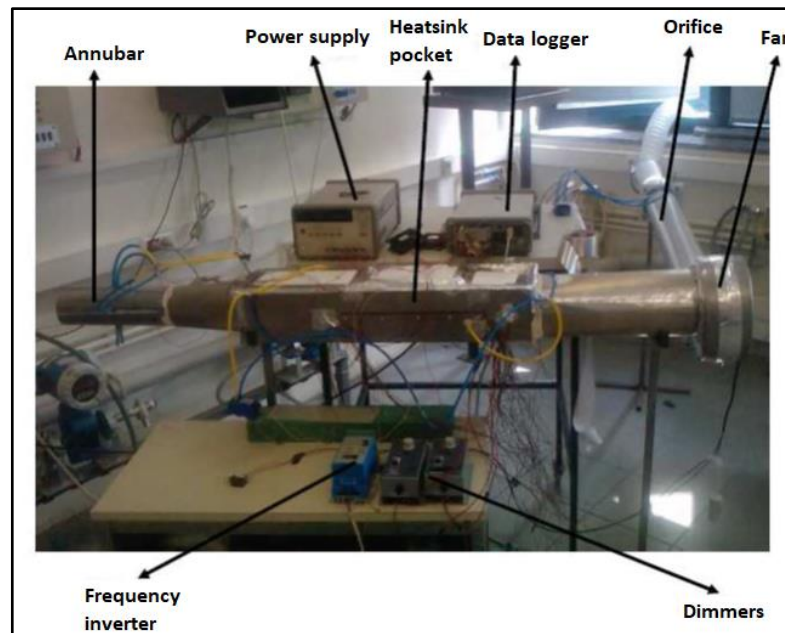
Figure 3.14. Heatsink testing setup

All outer surfaces of the test setup are insulated. Two plate type heaters with the power of 120 W, shown in Figure 3.15, are selected for the setup. The smaller heater is placed under the insulation and the bigger heater is placed on the insulation in the heatsink pocket.

Figure 3.15. Plate type heaters

The surface of the primary heater is covered with thermal paste and a 15mm-thick copper block is placed on the covered surface to distribute the heat uniformly. Twelve thermocouples are placed on the copper block as shown in Figure 3.16 to measure the heatsink bottom surface temperature.
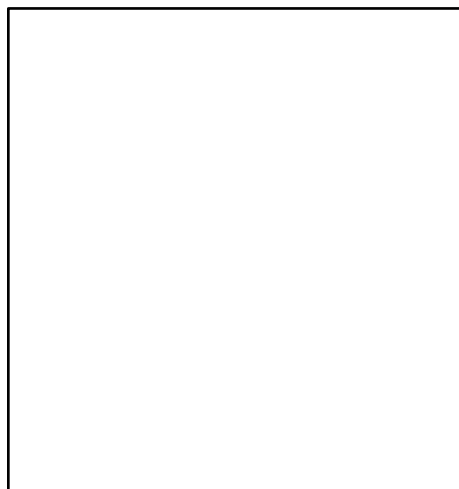
Figure 3.16. Copper plate and thermocouples

Thermal paste is applied to the copper block upper surface as well as to the heater surface to minimize contact thermal resistances. The heatsink test specimen is placed upon the copper block. In addition to the thermocouples on the copper block, six more thermocouples are instrumented to the heatsink bottom surface.

After placing the heatsink, pressure probes are installed in the system. Pressure taps are made on the setup walls close to the inlet and outlet of the heatsink, and pressure tubes are connected to these pressure taps. Pressure tubes are then connected to the both ends of pressure drop sensors with T-shaped fittings. Thermocouples are also placed inside of the channel downstream of flow straighteners to measure air temperature within the inlet and outlet of the heatsink.
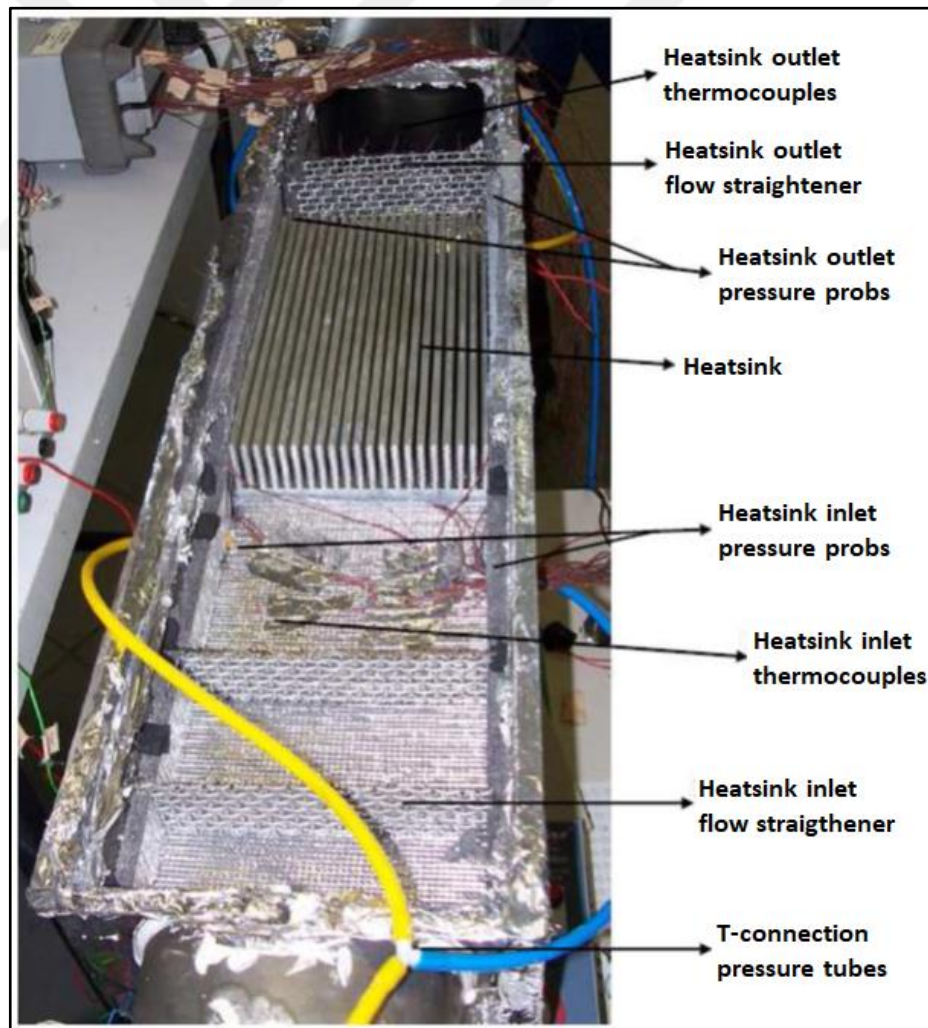
Figure 3.17. Components placement in heatsink pocket

An orifice is placed at the fan outlet and its air flow rate measurement is used as a double check with the annubar system. In addition to this, the heatsink test setup is equipped with a frequency inverter which enables to change the air flow rate and two dimmers which enable to adjust heaters powers separately. A data logger is used to record the data from the pressure drop sensors and thermocouples.

Figure 3.18. Orifice system

3.2.2. Experiments on Heatsink Test Setup

Heatsink performance is examined on the testing setup by measuring pressure drop and thermal resistance parameters. After the primary heater power and fan flow rate are set to the desired values, the secondary heater is powered to prevent heat loss from the primary heater. Measurements are made at steady-state conditions. The air flow rate is measured by the annubar.

The flow rate measured by the annubar is double checked by the orifice meter which is positioned downstream of the fan in the system. Pressure drop $(p_1 - p_2)$ across the orifice is measured and the air density (ρ) is calculated as a function of air temperature. Thus, air flow rate (Q) is calculated using the equation below.

$$Q = C_0 Q_{ideal} = C_0 A_0 \sqrt{\frac{2(p_1 - p_2)}{\rho(1-\beta^4)}} \tag{3.1}$$

The orifice discharge coefficient C_0 is calculated as a function of Reynolds number and the ratio of the orifice diameter to the pipe diameter (β) as shown in Figure 3.19.
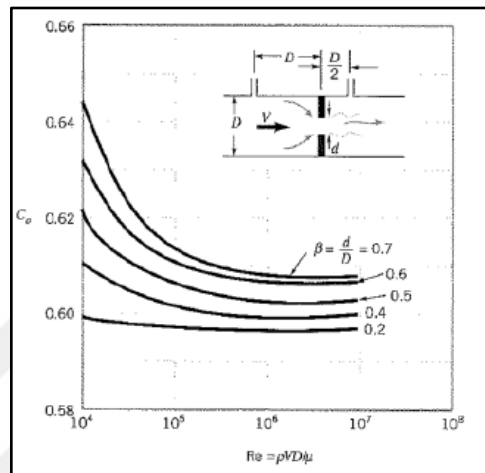
Figure 3.19. Orifice flow rate measurement

During the feasibility study of the hybrid system, the maximum allowable hot side heatsink thermal resistance value is calculated to be 0.02°C/W (K/W). After searching for the catalogues of various heatsink suppliers, an AMS Technologies production heatsink is selected for the experiments. The heatsink with the dimension of 150x120mm has the thermal resistance of 0.035°C/W at the flow rate of 60 l/s.
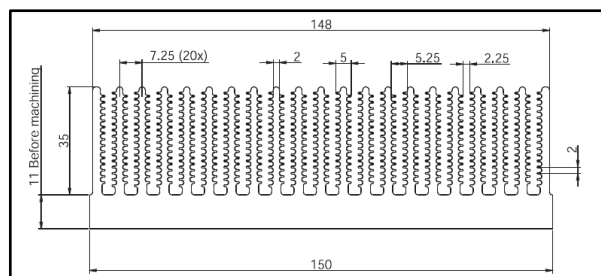
Figure 3.20. Selected heatsink fin geometry
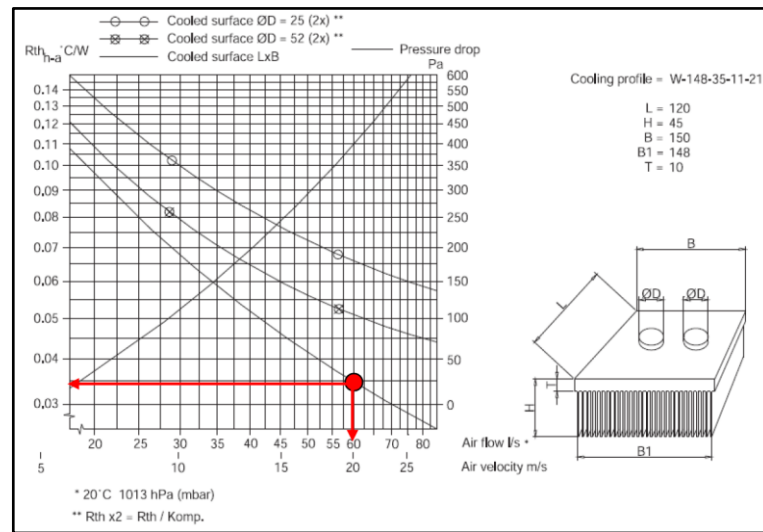
Figure 3.21. Selected heatsink performance graph and dimensions

The thermal resistance and pressure drop of the heatsink can be reduced by enlarging its dimensions according to the calculations. Since the dryer allows the maximum space of 250x250mm for a thermoelectric module, a larger heatsink has been employed in the experiment. As a result, the heatsink performance becomes better than the target with the new dimensions.
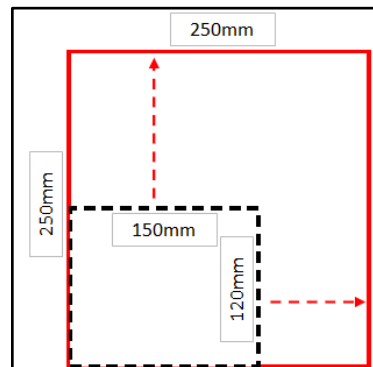
Figure 3.22. Selected heatsink re-dimensioning

- Thermal resistance (Rth) & thermal conductivity (UA) with new dimensions:

$$^1/_{UA} = R_{th} = 0.035/(L_{250}/L_{120}) = \mathbf{0.0168\ °C/W},\ \mathbf{UA = 59\ W/K} \qquad (3.2)$$

Since different flow rates can be achieved by adjusting the fan frequency, it is not necessary to enlarge the width of the selected heatsink. Therefore, the test setup employs the heatsink with the size of 250x150mm by increasing its original length from 120mm to 250mm. Pressure drop versus flow rate curve of the heatsink is shown in Figure 3.23.
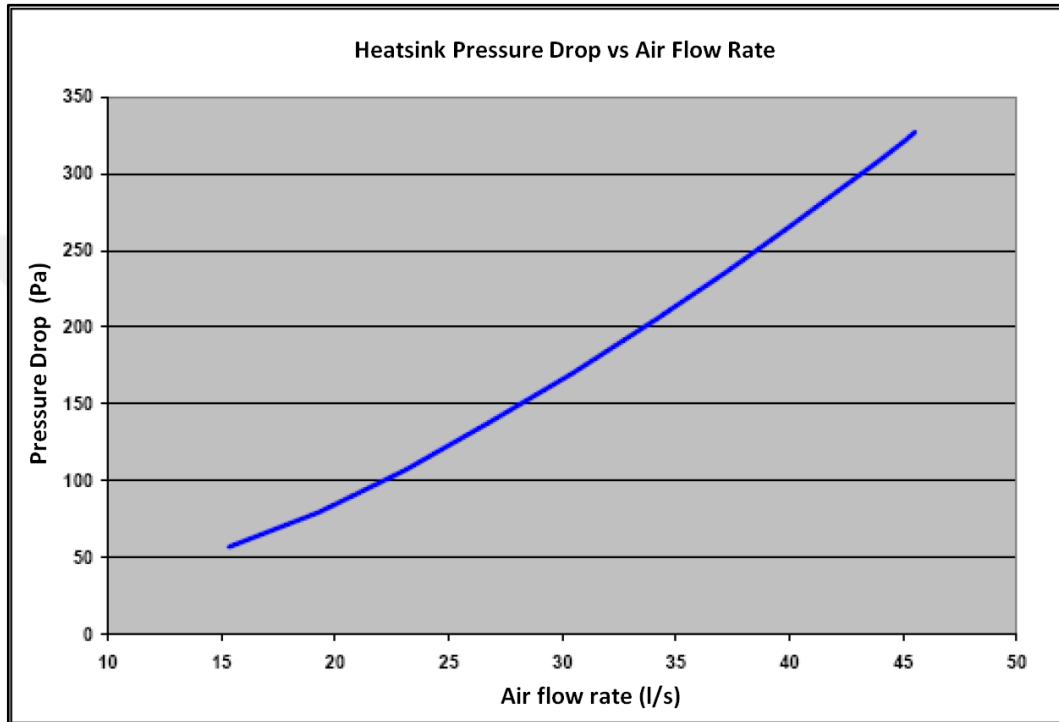
Figure 3.23. Heatsink pressure drop vs air flow rate

Heatsink inlet and outlet air temperatures and bottom surface temperatures are measured in steady-state conditions by thermocouples and are used to calculate the heatsink thermal resistance (R_{th}) using formulas shown below.

$$ {^1}/_{UA} = R_{th} = \frac{\Delta T}{Q} \tag{3.3} $$

$$ \Delta T = T_{bottom_{ave}} - \left(\frac{T_{in_{ave}} + T_{out_{ave}}}{2} \right) \tag{3.4} $$

$$ Q = \dot{m}_{air} C_{p_{air}} \left(T_{outlet_{ave}} - T_{inlet_{ave}} \right) \tag{3.5} $$

The performance of the heatsink provided from AMS Technologies is shown in Figure 3.24 where thermal resistance and pressure drop are plotted as a function of air flow rate.
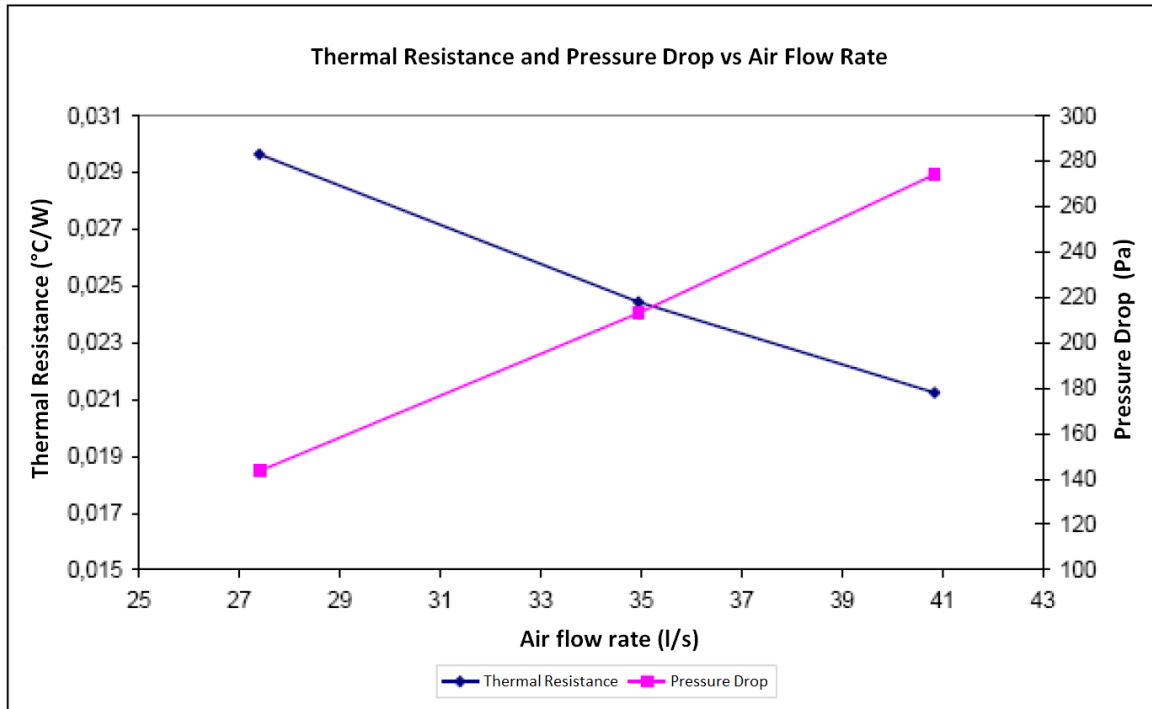
Figure 3.24. Thermal resistance and pressure drop as a function of air flow rate

Now that the heatsink selection is made and its performance measurements are completed in the heatsink testing setup, this test setup is available for further performance measurements on alternative heatsinks. In the next section, the thermoelectric system performance is examined with the selected hot side heatsink design at the Condenser Test Setup (CTS).

3.3. SUBSEQUENT CTS RESULTS

The selected heatsink is placed at the Condenser Test Setup for the second CTS test. Another heatsink which has 1.2mm fin thickness and 3mm fin gap is used as coldsink. The thermoelectric module is prepared with 150mm width due to the CTS structure restrictions. Thermal resistance values are calculated from the cooling power which is calculated by the TEC calculation tool. These thermal resistance values of the tested heatsink are

extrapolated to the thermal resistances of heatsinks that would have the maximum dimension allowed for the actual dryer machine.
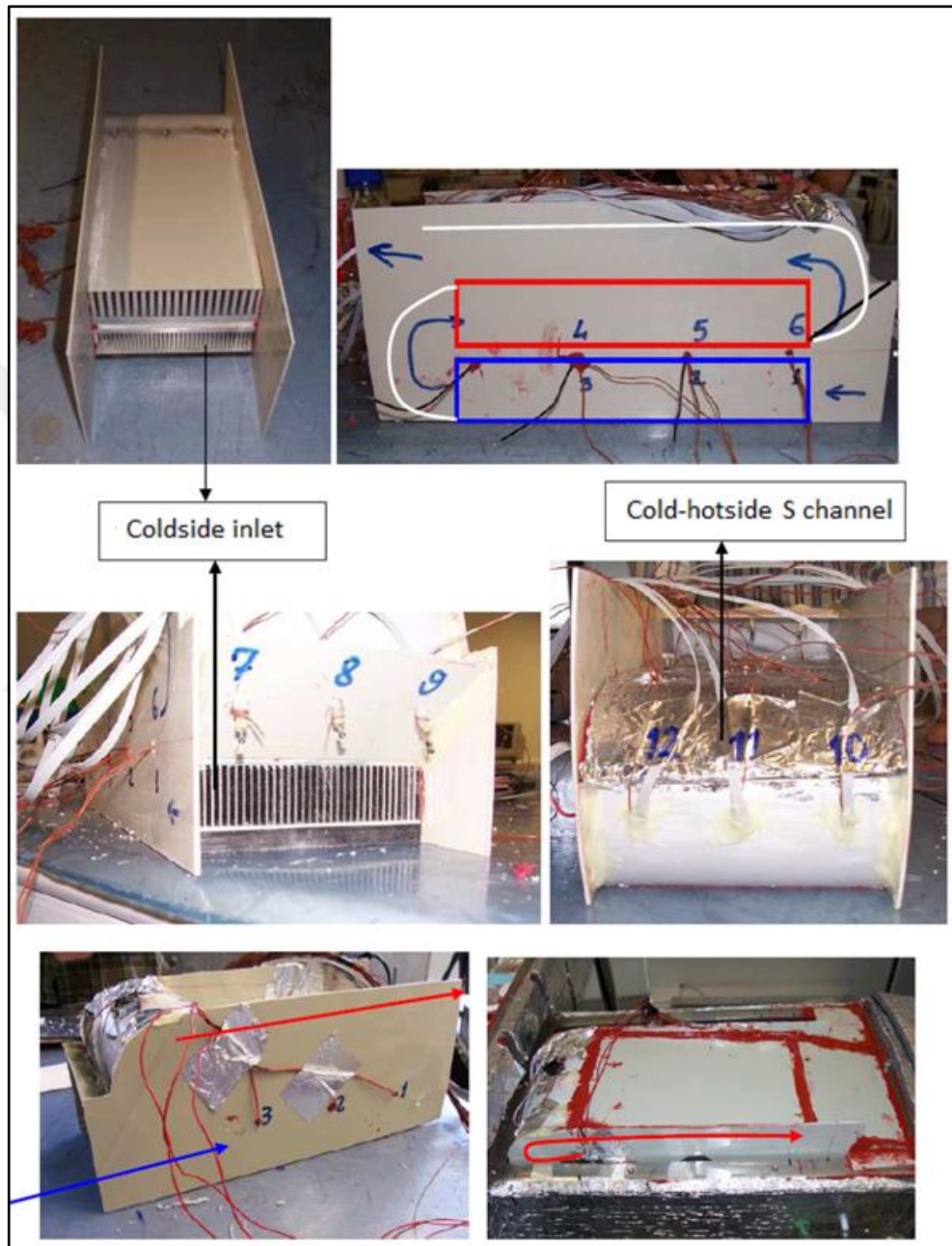
Figure 3.25. Secondary thermoelectric module instrumentation and CTS application
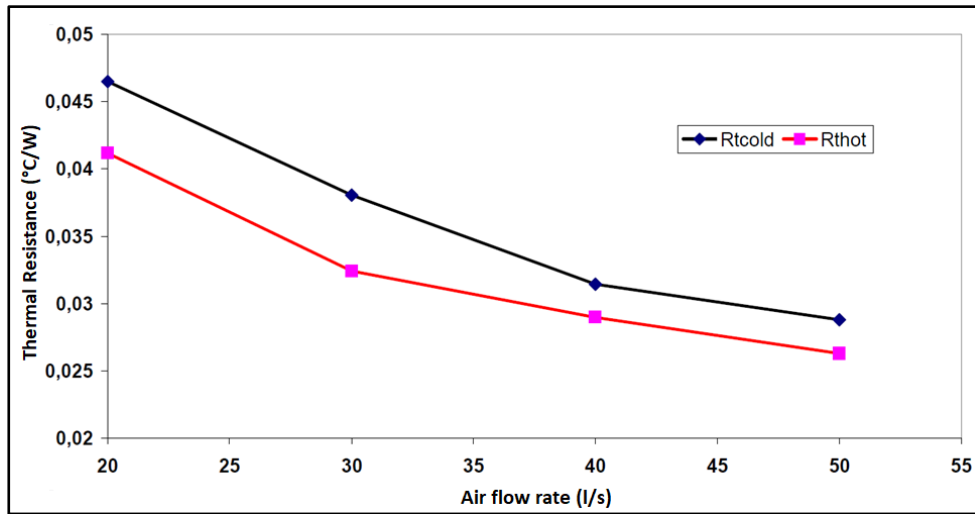
Figure 3.26. Cold and hot side thermal resistance measurements on CTS (width=150mm)
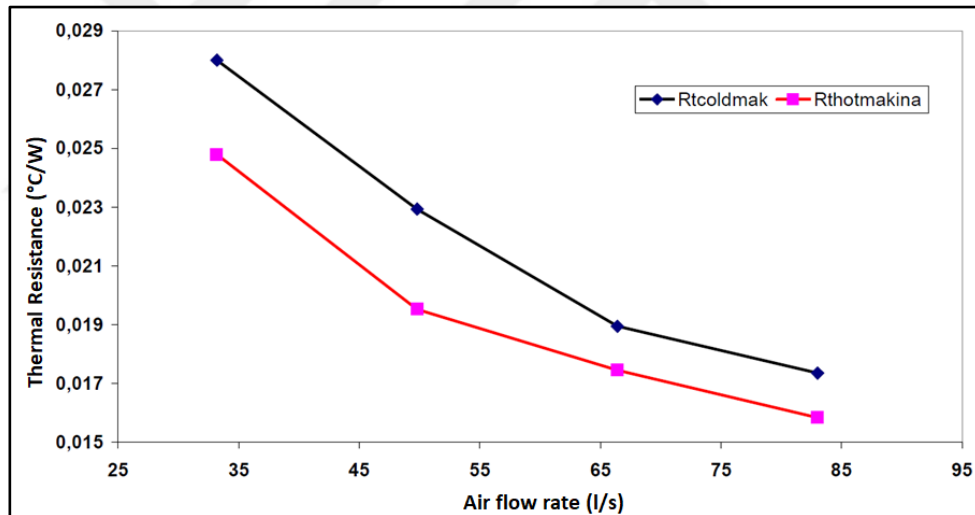
Figure 3.27. Cold and hot side thermal resistance values extrapolated to dryer machine dimensions (width=250mm)

The thermal resistance value of the selected heatsink with 250mm length is measured to be 0.018°C/W at the air flow rate of 60 l/s at CTS tests. The catalogue value of 0.0168°C/W is not achieved during CTS tests because performance values on the catalogue assume the 100 per cent usage of the heatsink bottom surface for the heat conduction which is not possible in the current thermoelectric module system due to the thermoelectric module arrangement. This performance degradation is taken into consideration in the hybrid dryer feasibility study.

In CTS experiments, the effect of thermoelectric module power is examined at the process flow rate of 35 l/s. The result shows that the higher voltage supplied to the modules, the higher temperature differences between the cold and hot sides of thermoelectric modules. The higher supply voltage also results in a higher heating power in the hot side and a higher cooling power in the cold side. For example, as the supply voltage increases from 10V to 12V, the cooling power increases from 280W to 310W while the heating power increases from 505W to 625W (see Figure 3.28). Therefore, it is evident that the supply voltage influences the heating power more than the cooling power.

The effect of thermoelectric modules power supply voltage on COP value is shown in Figure 3.29. It is shown that COP value decreases with increasing voltage and temperature difference between the cold and hot surfaces of the modules.
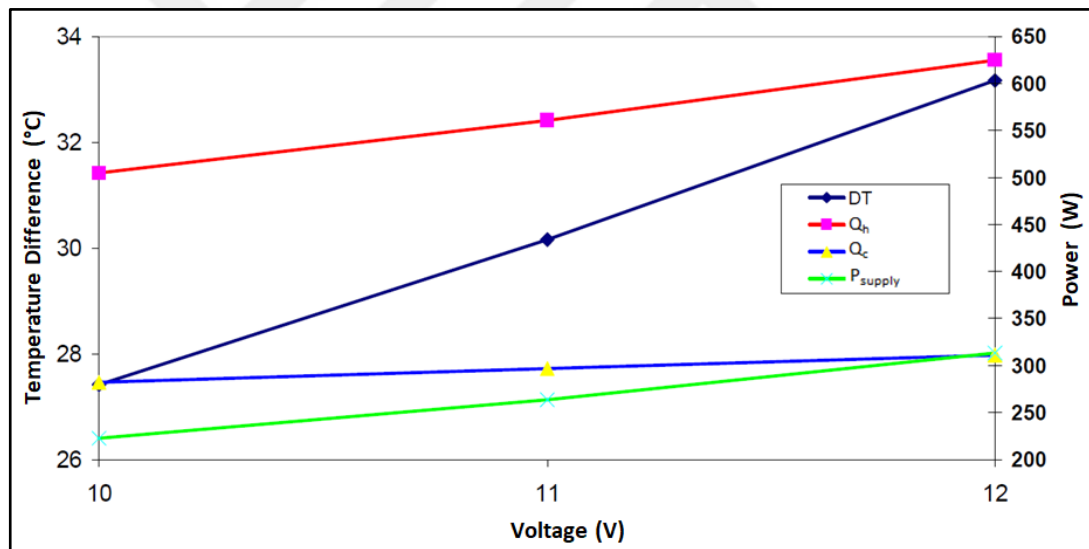
Figure 3.28. Thermoelectric module voltage effect on Q_h, Q_c and DT
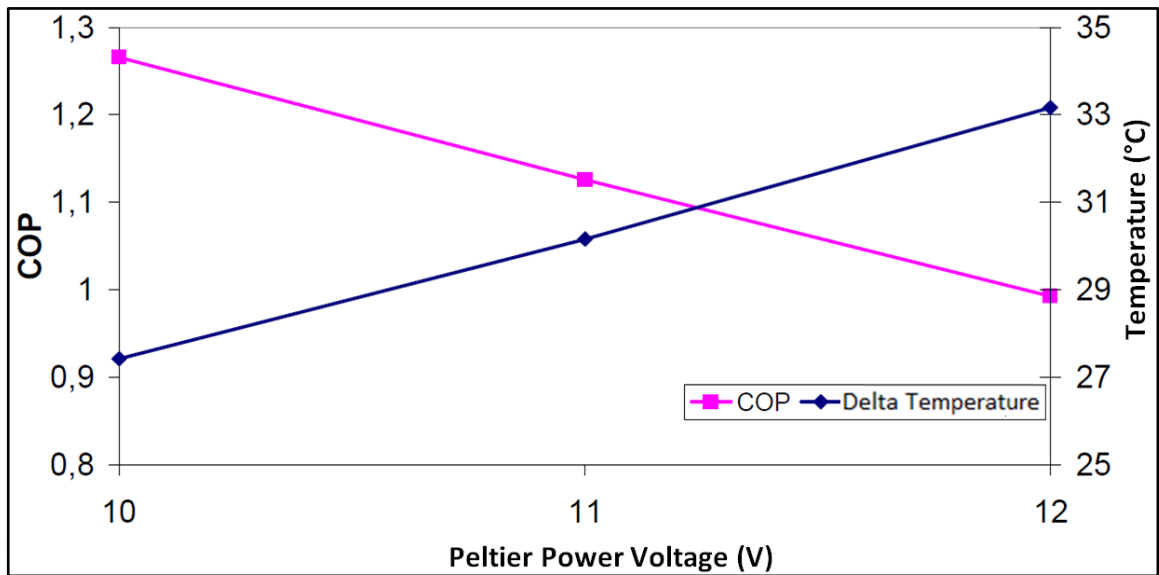
Figure 3.29. Thermoelectric module voltage effect on DT and COP

In order to see the effect of air flow rate on COP and Q_c, additional experiments are conducted at CTS with constant thermoelectric module voltage and different flow rates. Figure 3.30 shows that Q_c and COP increase as the process air flow rate increases.
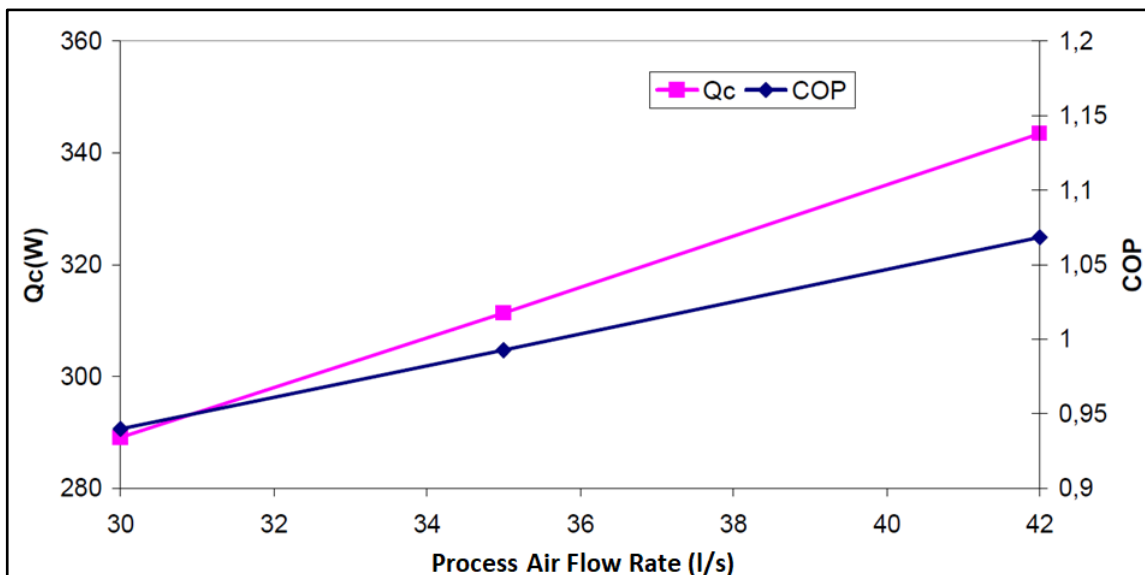
Figure 3.30. The effect of process air flow rate on Qc and COP

4. HYBRID TUMBLE DRYER EXPERIMENTS

Condenser tumble dryer of B-level specific energy consumption is assumed as "REF" in hybrid dryer feasibility calculation. In this calculation, COP of thermoelectric system is assumed as 0.85 which is obtained during CTS tests. As a result of the calculation, it appears that A-level specific energy consumption can be achieved when the electrical circuit efficiency is 85 per cent. If the electrical circuit efficiency is assumed to be 100 per cent, 4 per cent better specific energy consumption would be reached.

Table 4.1. Hybrid dryer system specific energy consumption calculation results

Assumptions	Values
Condenser Dryer SE	REF*
Electrical Heater Power	2500 W
COP	0.85
Peltier Heating Power	1000 W
Peltier Cooling Power	460 W
Electric Motor Power	200 W
Tumble Capacity	8 kg

Electrical Efficiency	SE
100%	0.853 REF*
95%	0.865 REF*
90%	0.876 REF*
85%	0.89 REF*

Hot and cold side heat exchangers are the parameters that affect the thermoelectric system performance most. Therefore, the geometric dimensions of these heatsinks are selected as large as possible to have lower thermal resistance and higher process air flow rate. The thermoelectric system of S-shaped serial air flow geometry with 3 layers is implemented to the hybrid dryer application due to the dimensional restriction and patent protections. Figure 4.1 shows the placement of the thermoelectric system with selected and re-dimensioned heatsinks inside of the dryer chassis. In this configuration, the condenser is also re-dimensioned with reduced length and increased width.
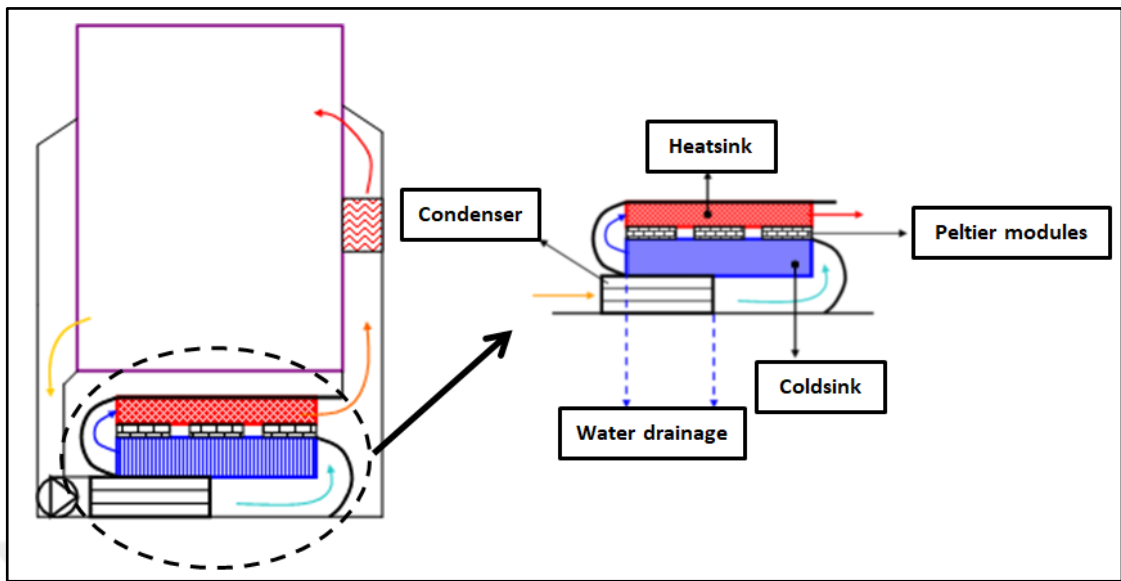
Figure 4.1. Hybrid system prototype configuration

4.1. THE FIRST PROTOTYPE

An existing heat pump dryer chassis is modified to accommodate the larger thermoelectric system and a high pressure radial fan. The prototype chassis is also modified to add additional cooling channel with air-cooled condenser and a cooling fan since a heat pump dryer does not have these features.

Figure 4.2. Thermoelectric modules arranged on the coldsink
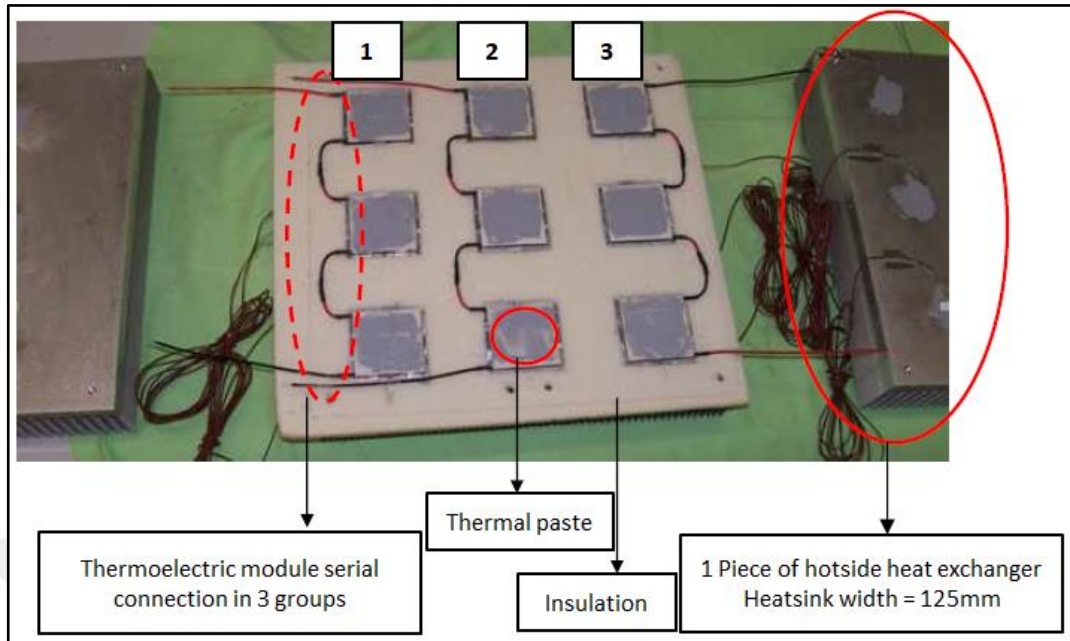
Figure 4.3. Thermoelectric system electrical connections, insulation and two heatsinks

As shown in Figure 4.3, nine thermoelectric modules are connected to each other in three groups and placed on the coldsink (cold side heat exchanger). Thermoelectric modules are powered with power supply units. Thermoelectric modules are fixed in their positions on the coldsink surface. Thermal paste is applied to both cold and hot surfaces of thermoelectric modules. Two heatsinks (hot side heat exchanger) are used with 125mm width due to the manufacturer limitations. The gaps between thermoelectric modules are insulated and heatsinks are assembled on the coldsink with the thermoelectric modules sandwiched in between.
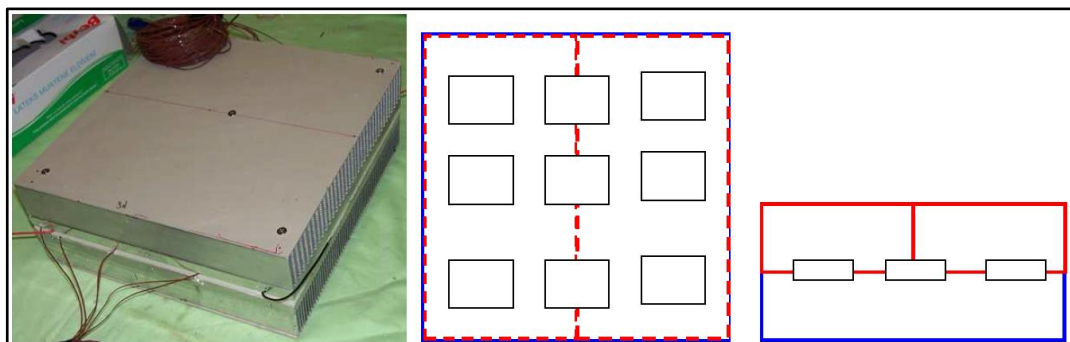
Figure 4.4. Thermoelectric system heatsink and coldsink assembly
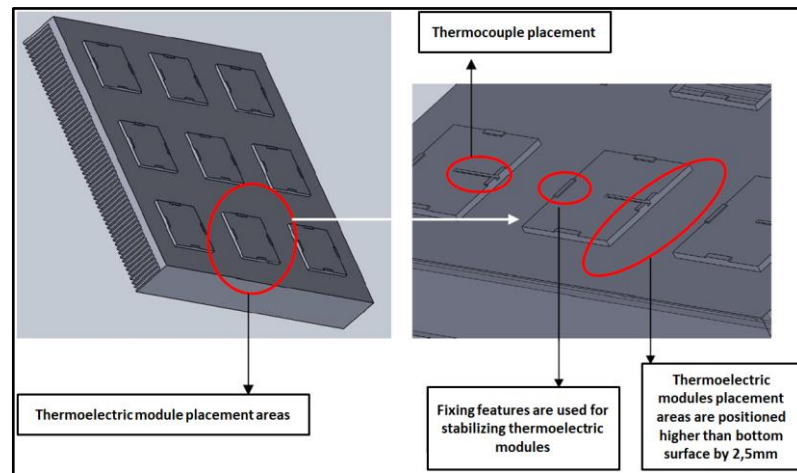
Figure 4.5. Thermoelectric modules placement and assembly

Figure 4.5 shows that the coldsink bottom surface is slightly cut out for the stable placement of thermoelectric modules. Fixtures are also added to the placement areas to allow no module movement during the operation.

Table 4.2. Coldsink features and dimensions

Coldsink Features	Dimensions
Width X length	250 mm X 250 mm
Coldsink surface area	0.0625 m^2
Peltier surface area	0.0144 m^2
Fin height	30 mm
Bottom thickness	10 mm
Fin thickness	1.2 mm
Fin gap	3 mm
Fin number	59
Total heat transfer surface area	0.97 m^2
Perpendicular edge surface area	0.0054 m^2

An existing air-cooled condenser which is used in Arçelik tumble dryers is modified for this prototype. As it is seen in Figure 4.6, the condenser height is reduced by eliminating two channels. Its length is decreased from 250mm to 140mm while its width is increased from 180mm to 250mm.
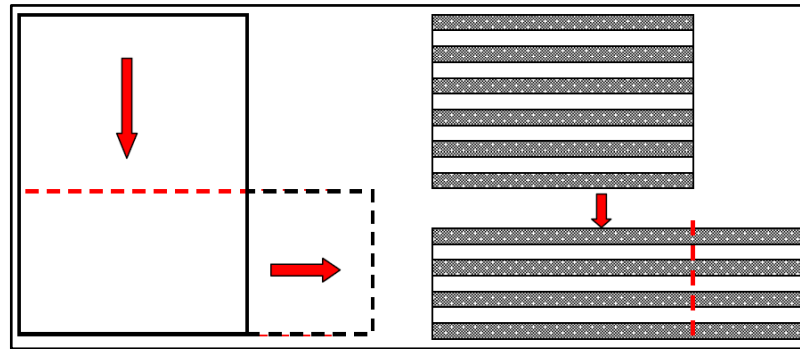
Figure 4.6. Condenser re-dimensioned for the hybrid dryer prototype

Figure 4.7. View of the condenser in the first prototype

Condenser space on side walls

S turns on side walls
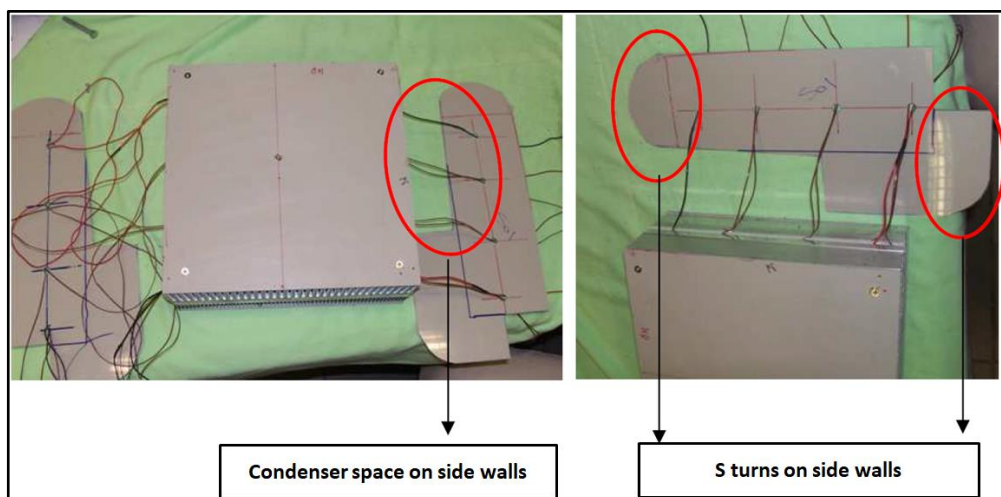
Figure 4.8. Thermoelectric system sidewalls with 180-degree elbows

Process air flow channels need to be built before assembling the thermoelectric system into the hybrid dryer prototype. Sidewalls shown in Figure 4.8 are produced for this purpose. Sidewalls are dimensioned to provide sufficient spaces for the condenser outlet and 180-degree elbows. Sidewalls and elbows are assembled as shown in Figure 4.9. A small gap is left on the lower side of elbow connecting the coldsink outlet and the heatsink inlet in order to collect the condensed water into the reservoir.
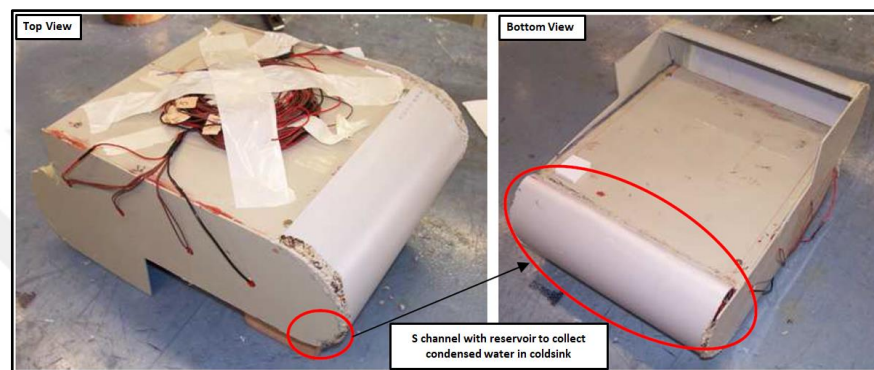
Figure 4.9. Thermoelectric system assembly with 180-degree elbows

The complete thermoelectric system assembly in the hybrid dryer machine prototype is shown in Figure 4.9. The thermoelectric system is placed on top of the air-cooled condenser. After leaving the tumble, damp process air passes through the condenser and then into the coldsink following 180-degree elbow channel. After it leaves the coldsink, it is directed to the heatsink by another 180-degree elbow channel. Moisture in the process air is condensed in both the air-cooled condenser and the cold side of thermoelectric system. Afterwards the process air is heated at the hot side of the thermoelectric system.

4.1.1. The First Prototype Experiments

After the first prototype of the hybrid dryer machine is built, pressure drop and process air flow rate are measured as shown in Figure 4.10. The total system pressure drop is 800 Pa for 50 l/s flow rate and 1200 Pa for 60 l/s. During these flow rate measurements, the fan power is also measured for different frequencies as shown in Figure 4.11 where the fan power is plotted against the flow rate.
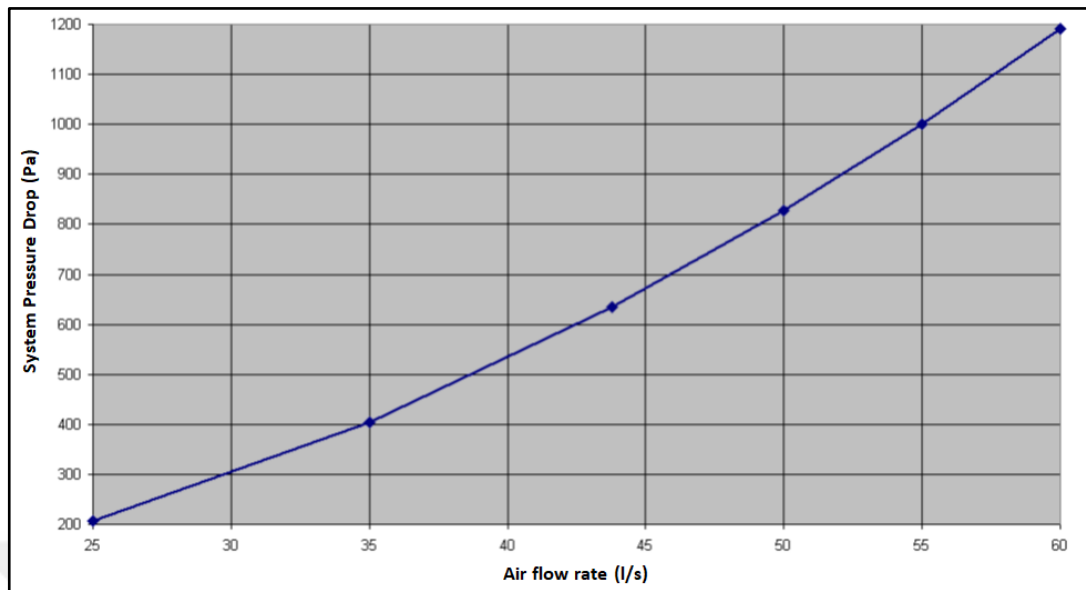
Figure 4.10. First prototype system characteristics
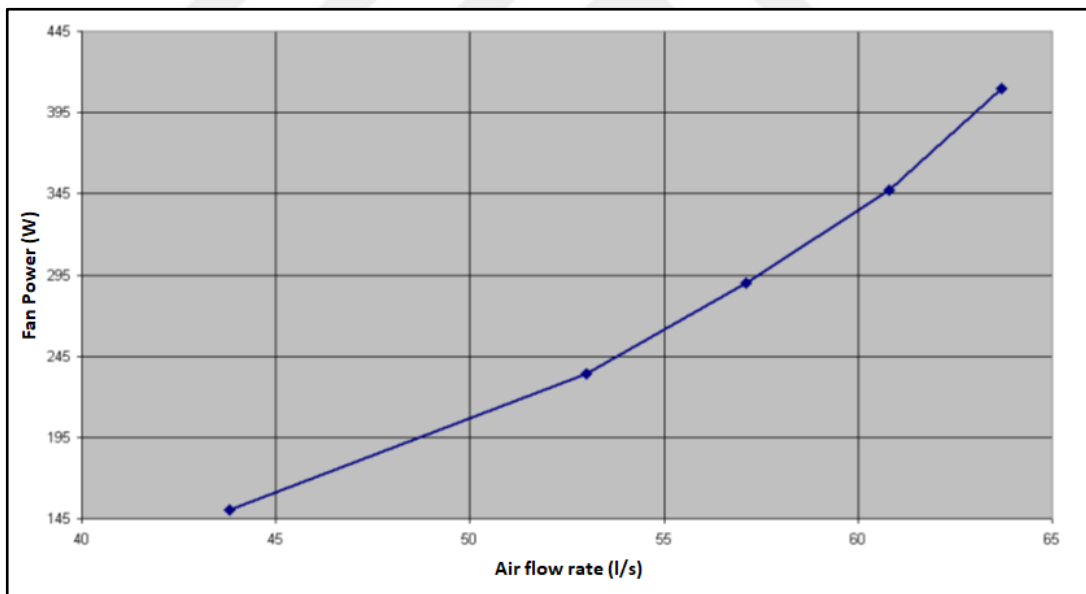
Figure 4.11. Fan power vs process air flow rate

The experiment setup for the first prototype is shown in Figure 4.12. The machine is placed on top of a platform in order to measure the condensation rates from the condenser and the thermoelectric system. Condensation pots and scales are placed under the platform in order to collect the condensate.

Figure 4.12. First prototype experiment setup

There are three different DC power suppliers to provide power for each thermoelectric group. DC voltage is measured from the power supply input. Electrical currents of thermoelectric modules are measured by the help of capacitors that are serially connected to the circuit.

After the initial experiments, it is found that there is high heat loss on 180-degree elbow channel at the coldsink inlet and thus insulation needs to be applied on it. Furthermore, it is also found that the front seating of the tumble is not sealed well. Therefore, additional insulation is applied to the channel at the coldsink inlet and the front tumble seal is thickened. As a result, the energy consumption is reduced by two per cent as shown in Table 4.3.
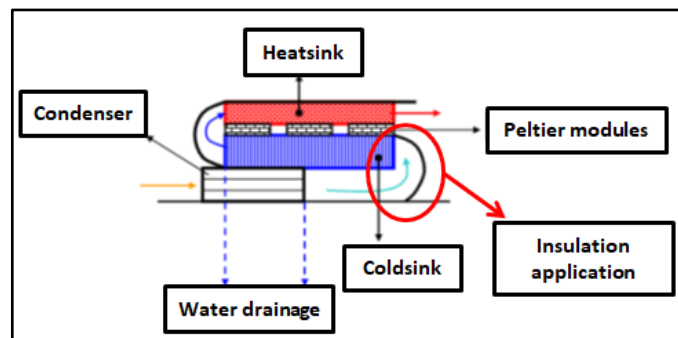
Figure 4.13. Insulation application at coldsink inlet

Table 4.3. Improvement actions effect on specific energy consumption of first prototype

SE wrt REF*	Laundry weight after operation (kg)	Moist percentage after operation (%)	SE consumption improvement (kWh/kg)		Improvement Actions
0.968 REF*	8.360	3.851	1%		Front seating seal thickened
0.966 REF*	8.310	3.681			
0.959 REF*	8.330	3.478		2%	
0.96 REF*	8.290	3.496	1%		Coldsink inlet insulation
0.954 REF*	8.235	2.937			
0.949 REF*	8.265	2.991			

The effect of increasing cooling air flow rate is also examined in additional experiments. It has been found that higher cooling air flow rate is increasing the amount of water condensed in the condenser but decreasing the amount of water condensed in the thermoelectric cold side.
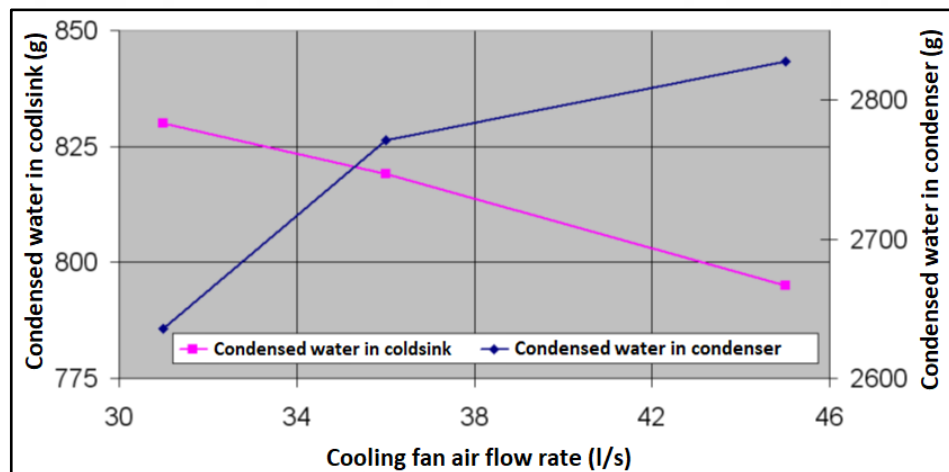
Figure 4.14. The effect of cooling air flow rate on the condensation in thermoelectric system and condenser

The final results of the experiments from the first hybrid dryer prototype are shown in Table 4.4. The moist percentage that remains in clothes at the end of the operation does not meet the standard specification which is between -3 and +3 per cent. Therefore, this specific energy consumption is not acceptable according to the standard labeling system.

Table 4.4. First prototype specific energy consumption result

SE wrt REF*	Moist percentage after operation (%)	Condensed water in coldsink (kg)	Condensed water in condenser (kg)	Water collection efficiency (%)
0.944 REF*	3.812	0.79	2.574	74.839

After the experiments performed with S-shaped serial air flow geometry with three layers, it is decided to implement a by-pass configuration to the thermoelectric system as shown in Figure 4.15. Consequently, the flow rate is reduced through the condenser and coldsink while the total process flow rate is improved with the by-pass application.
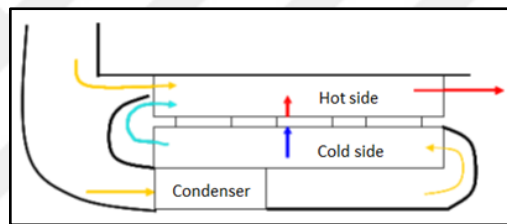
Figure 4.15. First prototype with by-pass application

The experimental results with the by-pass application on the first hybrid dryer prototype is shown in table 4.5.

Table 4.5. First prototype experiment results after by-pass application

SE wrt REF*	Condensed water in coldsink (kg)	Water collection efficiency (%)
0.924 REF*	0.861	75.08
0.937 REF*	0.805	75.97
0.924 REF*	0.831	76.29

After the by-pass application, the specific energy consumption is improved by 7.6 per cent and the water collection efficiency is measured to be 76 per cent for the first prototype of hybrid dryer.
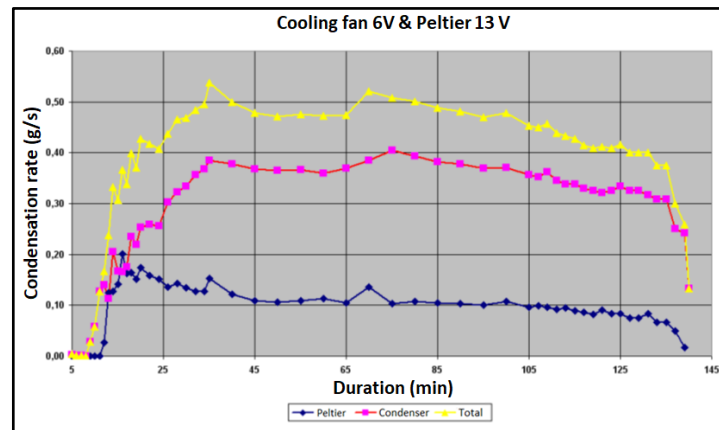
Figure 4.16. First prototype condensation rate for thermoelectric system and condenser

Condensation rates measured at the first prototype are shown in Figure 4.16. During the steady-state operation, condensation rate is approximately 0.1 g/s in Peltier modules and 0.4 g/s in condenser, and thus the total condensation rate is around 0.5 g/s.
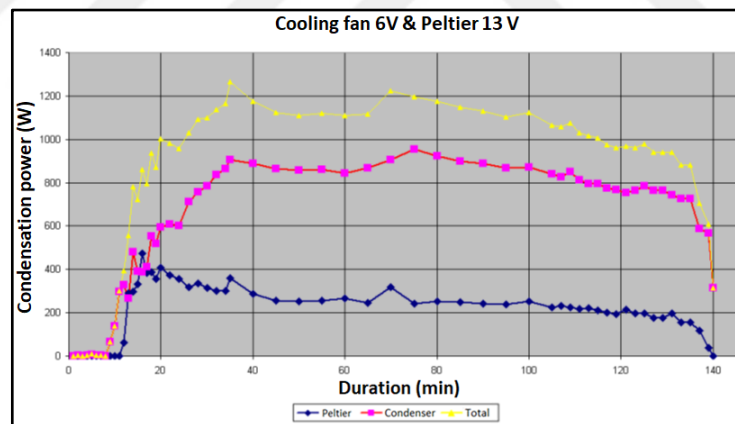
Figure 4.17. First prototype condensation energy

As discussed in Section 2.3, the cooling power that is absorbed from the cold side of the thermoelectric system is an important parameter for achieving the target specific energy consumption. Note that water condensation takes place at the cold side of thermoelectric system, and that the heat recovery of the thermoelectric system is closely related to the condensation power provided by the cold side. First prototype condensation energy that is recovered from the condenser and thermoelectric system is shown in Figure 4.18. The total energy recovered from the thermoelectric system is 235 W.
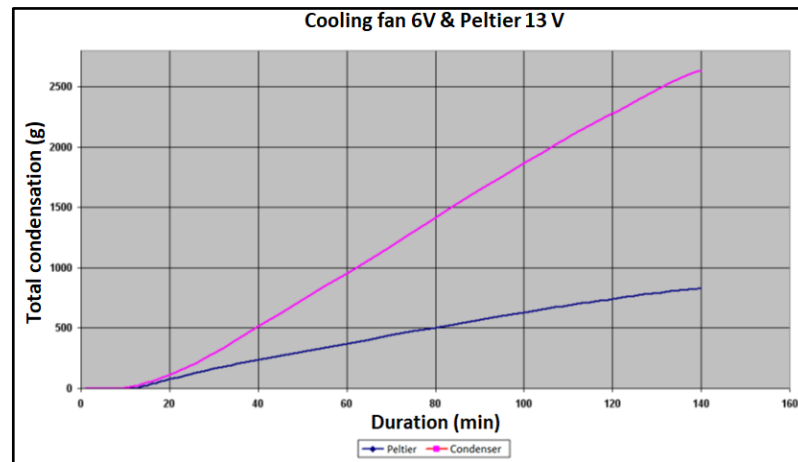
Figure 4.18. First prototype condensation curves for thermoelectric system and condenser

4.1.2. The First Prototype Problems

Several factors that affect the failure on achieving the specific energy consumption target with the first hybrid tumble dryer prototype are discussed in this section.

4.1.2.1. Process Air Leakage Effect

Sealing issues are detected in front and rear tumble seating areas of the first prototype. Additional seals are added to the rear tumble seating. Even though additional seals worked well during the initial tests, it is observed that the seals are deformed in time. Alternative seal usage is examined to overcome the leakage problem. [12]

4.1.2.2. Tumble Seating Effect

It is found out that the design of tumble seating in the first hybrid dryer prototype causes higher pressure drop at the inlet and outlet of the tumble. Roller support design is considered as a solution to improve the tumble motion during operation.

4.1.2.3. The Effect of Utilization of The Heatsink Bottom Surface Area

The total surface area of nine thermoelectric modules is only 23 per cent of the heatsink bottom surface area in the thermoelectric system. Therefore, the full capacity of the heatsink was not fully utilized. According to the heatsink performance graph that is provided by AMS technologies, heatsink thermal resistance increases from 0.035°C/W to 0.05°C/W as the contact surface ratio reduces from 100 per cent to 23 per cent. CFD analysis result also shows that the free spaces between Peltier modules have lower temperatures.
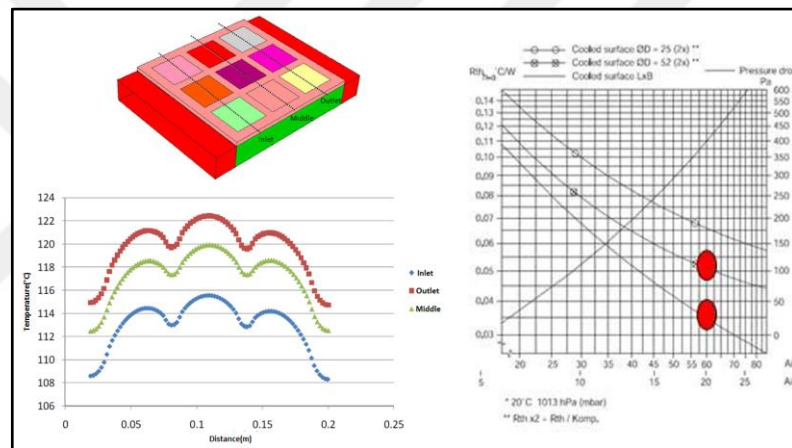
Figure 4.19. Heatsink surface area utilization effect

4.1.2.4. The Effect of Peltier Module Performance Variance Through The Flow

Temperature analysis on the thermoelectric modules shows that the temperature difference between the cold and hot side of the modules are increasing in the air flow direction at the hot side of thermoelectric system. The increase of temperature difference on the thermoelectric module surfaces causes performance degradation.
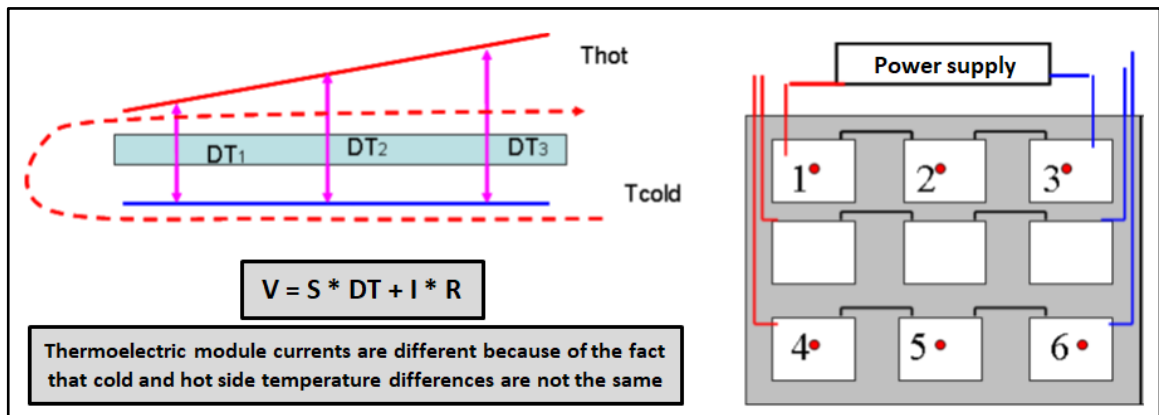
Figure 4.20. Thermoelectric system performance degradation through the flow

4.1.2.5. *The Effect of The Energy Stored in Heat Exchangers*

Heat exchangers made of aluminum blocks are used to increase heat transfer between thermoelectric modules and the process air. These aluminum components have huge thermal mass and store a significant amount of energy. When the system reaches to the thermal equilibrium during the operation, the heat exchanger temperatures of the hot and cold sides go up to 100°C and 60°C, respectively.
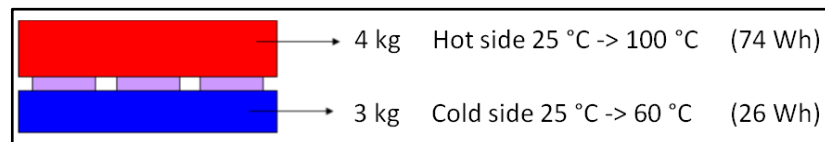
Figure 4.21. Energy stored in the heat exchangers

The amount of energies stored in the hot and cold side heat exchangers of thermoelectric system are calculated separately by using the thermal capacity of aluminum material. As shown in Figure 4.21, the total energy of 100Wh is stored in the heat exchangers, resulting in the increase of the specific energy consumption.

4.1.2.6. *Fiber Accumulation Problem*

Fiber accumulation is observed on both cold and hot side heat exchangers during the tear-down inspection of the first hybrid tumble dryer. It is found that the fiber accumulation is more intensive at the coldsink inlet. Fiber accumulation in the areas shown in Figure 4.22 causes the process air flow rate to be reduced. In addition, condensation performance in the cold side of thermoelectric system is also reduced as the fiber accumulation prohibits direct contact between the coldsink surface and the process air.
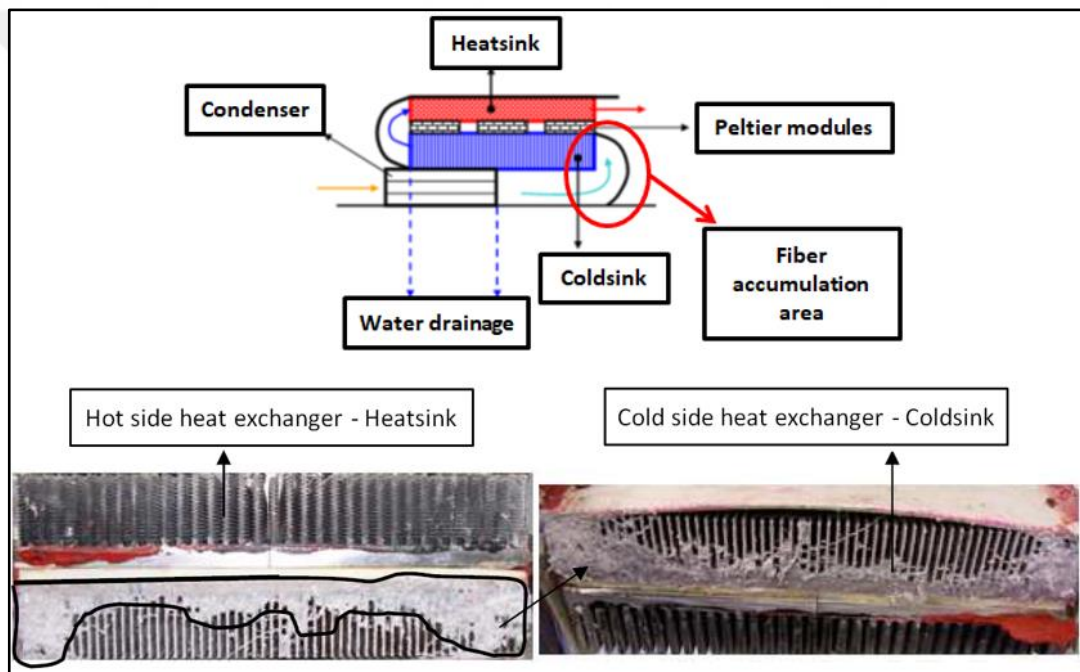
Figure 4.22. Heat exchanger fiber accumulation area

4.2. THE SECOND PROTOTYPE

In the first prototype experiments, it is found that the structural problems affect the hybrid dryer performance significantly. In the first prototype there is no roller support that reduces the load, causing the motor to spend more power to turn the tumble. Since the system pressure drop is also high in the first prototype, it requires high-power radial fan to obtain higher process air flow rate. This also causes sealing problems in operation. In the first prototype, the front tumble seating and the fiber filter are not desirable, too.

Therefore, some structural improvements on the chassis of the second hybrid dryer prototype are planned in order to have lower system pressure drop and higher process flow rate with a low-power process fan. However, any change in the thermoelectric system is not made in the second prototype to have a better understanding about the impact of structural improvements on the drying performance.

- Increased chassis height
- Optimized process channels
- Increased performance of the process fan
- Improved seals
- New front tumble seating and fiber filter
- New roller supports to the tumble

In the second prototype, roller tumble supports are applied to reduce load on the motor. Not only process channels but also cooling channels are modified due to the need of chassis bottom height change to place the thermoelectric system. Increase of allowable package from chassis modifications also helps to increase the condenser height in the second prototype. A condenser with 4 channels and 5 cooling channels is selected. The heights of each process channel and cooling channel are 9.0 mm and 5.5 mm, respectively.

No major modifications are made on the thermoelectric modules, heatsink and coldsink compared to the first prototype. The only change in the thermoelectric system is that 180-degree elbow channels are slightly extended to reduce pressure drop (see Figure 4.23).
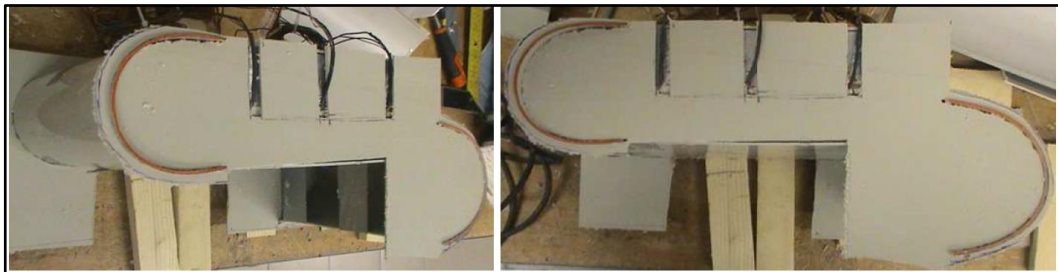
Figure 4.23. Thermoelectric system 180-degree elbows in the second prototype

4.2.1. The Second Prototype Experiments

Thermoelectric module performance is determined by the temperature data collected from thermocouples placed on the cold and hot sides of Peltier module surfaces. Both temperatures of the process air at the tumble outlet (door) and Peltier module cold surfaces are shown in Figure 4.24. Module surface temperatures are observed to be lower than the process air temperature at the tumble door from the beginning of the drying operation to the end. In the beginning of the drying operation, Peltier module surface temperatures are measured to be approximately 15°C while temperature at the tumble outlet is 23°C. Lower temperatures on the Peltier module surfaces result in condensation on the cold side surface of the thermoelectric system.
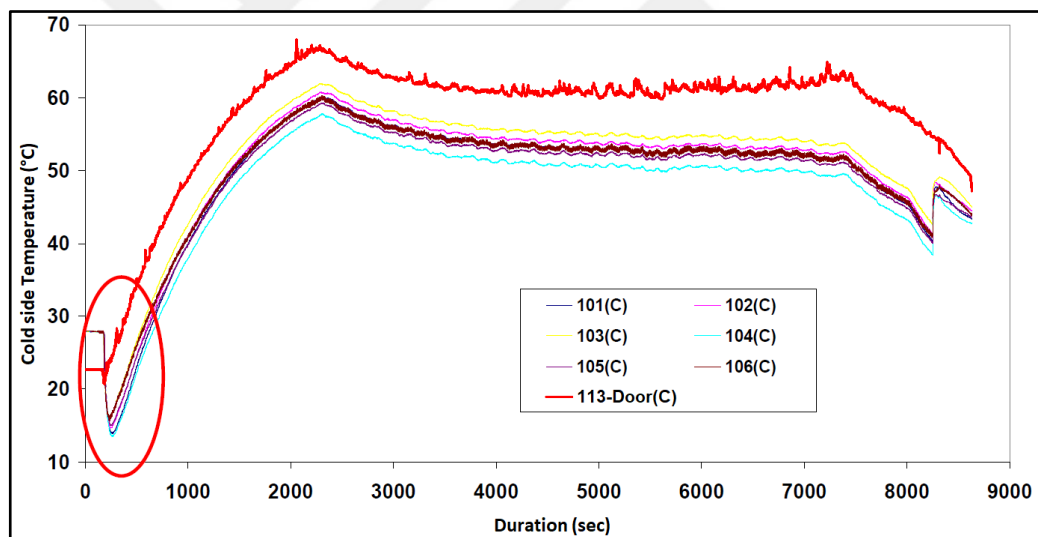
Figure 4.24. Cold side temperature measurements in the second prototype

The tumble door temperature is around 61°C in the steady-state region of the drying operation and the Peltier module cold surface temperatures vary from 50°C to 55°C. As shown in Figure 4.25, the thermoelectric module cold surface temperature decreases by only 2°C from the inlet to the outlet. Peltier module cold surface temperature decreases by 2.2°C in the left side and by 2°C in the right side from the inlet to the outlet.
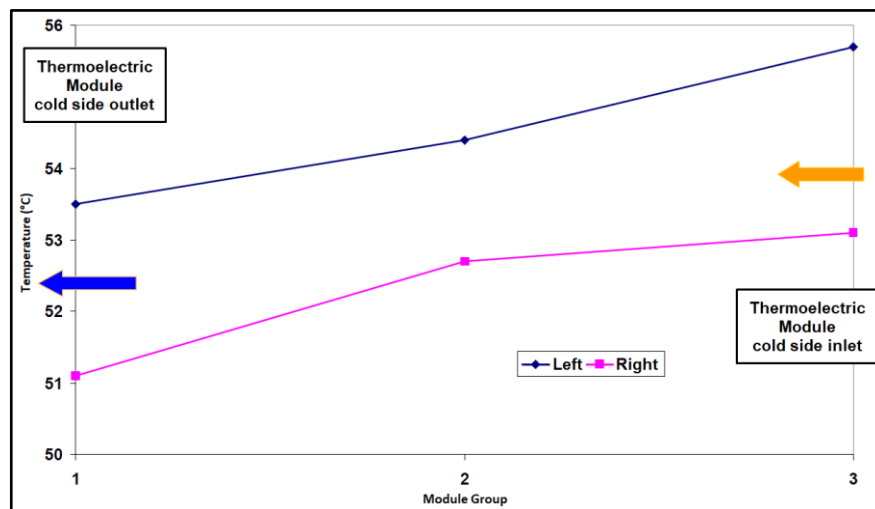
Figure 4.25. Peltier module cold surface temperature change through the flow
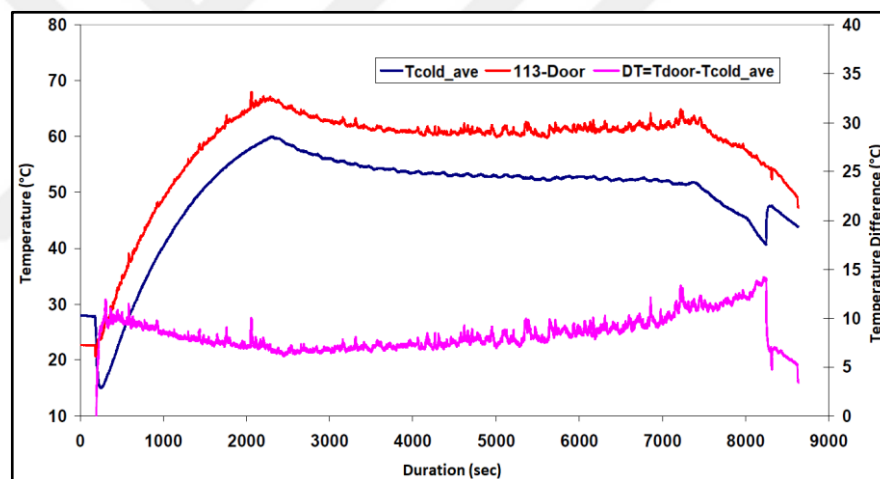
Figure 4.26. Comparison of tumble outlet (door) and Peltier module cold surface temperatures

Figure 4.26 shows the average temperature of thermoelectric module cold surfaces (left-side scale) and its difference to the tumble outlet temperature (right-side scale). It appears that the temperature difference between process air at the tumble outlet and thermoelectric module cold side comes down to its minimum value during the steady-state of drying operation. Toward the end of the drying operation, however, this temperature difference increases due to lower condensation rate on the cold side of the thermoelectric system.
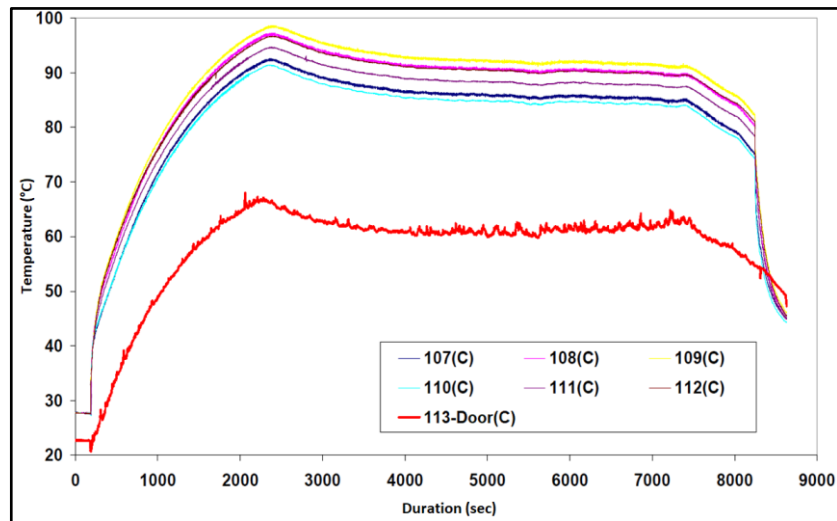
Figure 4.27. Temperatures of Peltier module surfaces and tumble outlet (door) in second
prototype
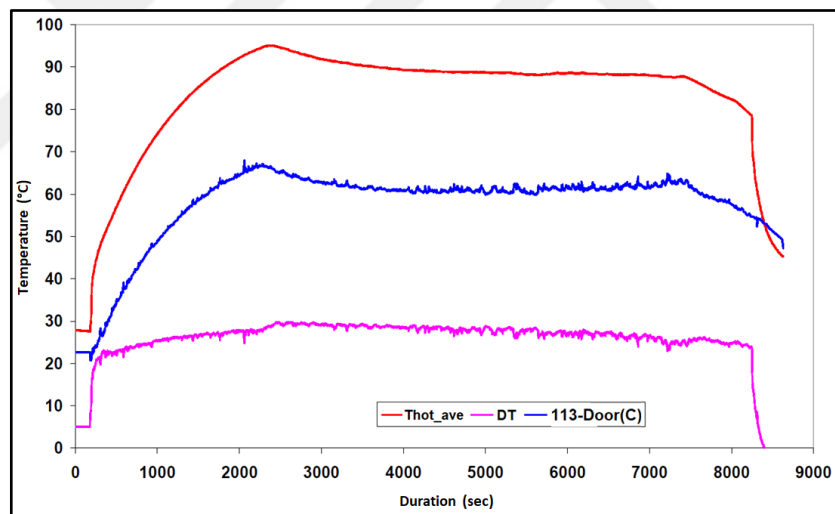
Figure 4.28. Comparison of temperatures at tumble outlet (door) and Peltier module hot
surface

Figure 4.27 and figure 4.28 show the temperatures of tumble outlet and thermoelectric
modules hot surfaces. It is found that the hot surface temperatures in thermoelectric system
are higher than the process air temperature at the tumble outlet from the beginning to the
end of the drying operation. Hot surface temperatures of the thermoelectric modules vary
from 92°C to 85°C during the steady-state drying operation.
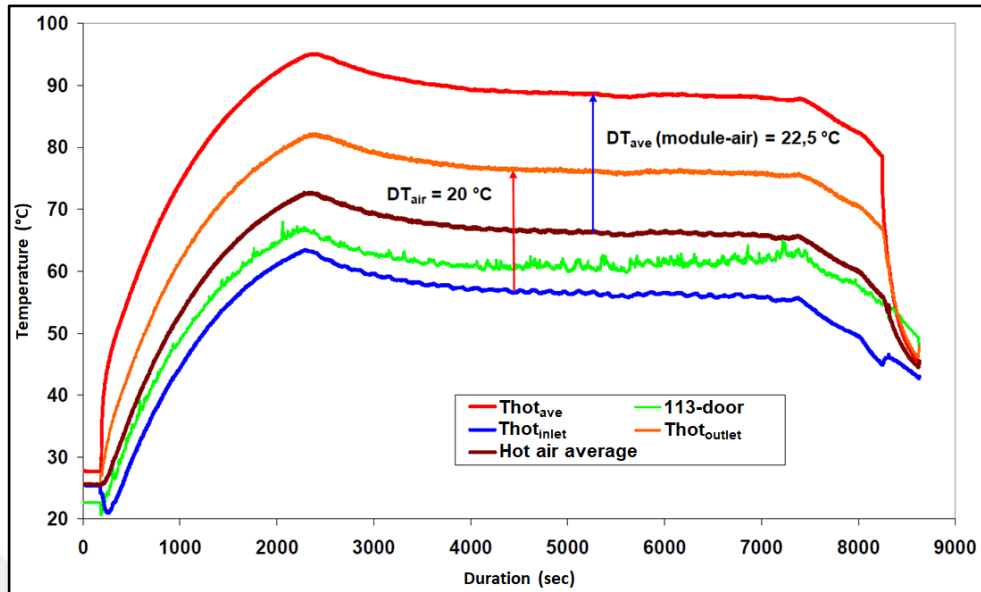
Figure 4.29. Temperature difference between the hot side surface and the process air

Figure 4.29 shows that the process air temperature increases by 20°C from the inlet to the outlet as the process air passes over the hot surface of the thermoelectric modules. The average temperature difference between the process air and the thermoelectric module hot surface is measured to be 22.5°C.
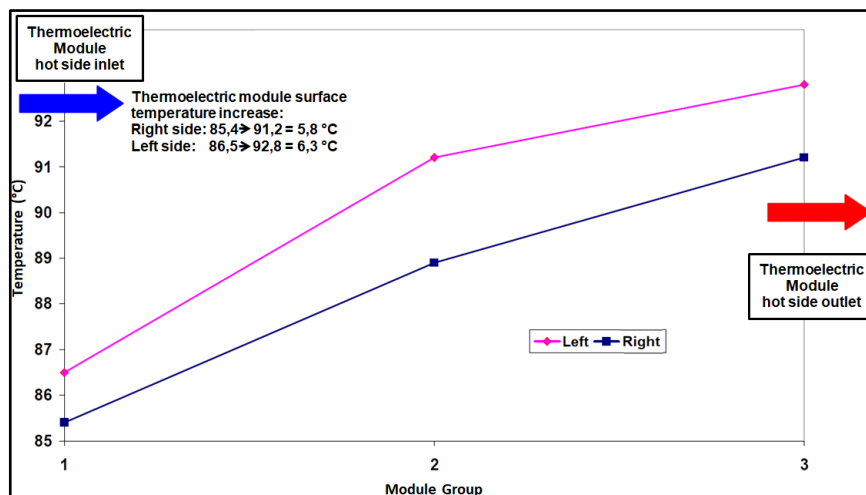
Figure 4.30. Peltier module hot side temperature change in the direction of process air flow during the steady-state operation

As shown in Figure 4.30, it is observed that thermoelectric hot surface temperatures increase in the process air flow direction and there is no significant difference between left and right side hot surface temperatures. When this data is compared with the cold side surface temperature differences shown in Figure 4.25, thermoelectric module cold surface temperatures decrease by 2°C in the direction of process air flow through the cold side of the thermoelectric system while hot surface temperatures increase by 6°C in the direction of process air flow through the hot side of the thermoelectric system.
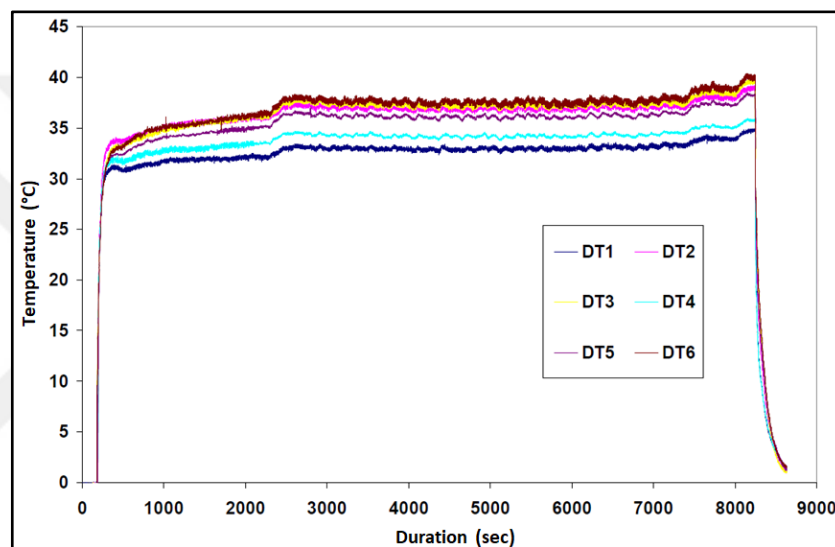
Figure 4.31. Peltier modules surface temperature differences

The temperature differences between the cold and hot surfaces of six Peltier modules out of nine in the thermoelectric system are examined in Figure 4.31. Thermoelectric module surface temperature differences are relatively smaller in the early transient state compared to the steady-state of the drying operation. The temperature differences increase even higher in the late transient state of drying operation.

Figure 4.32 shows that temperature difference between the hot and cold surfaces of the thermoelectric modules increases in the flow direction through the hot side of thermoelectric system. This means that the performance of the thermoelectric modules decreases in the process air flow direction through hot side.
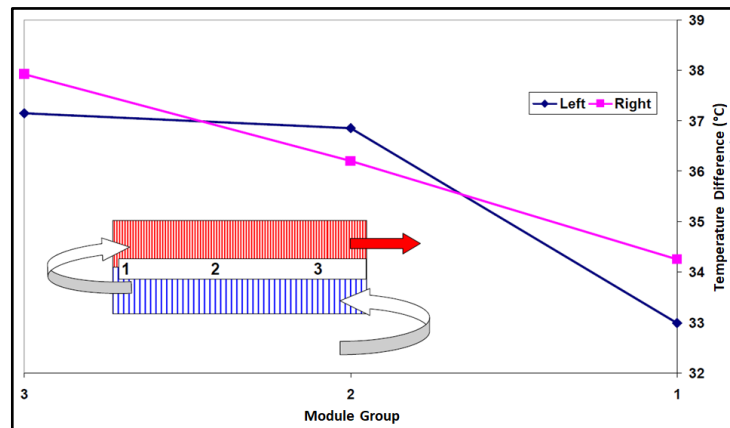
Figure 4.32. Thermoelectric module temperature differences through the flow
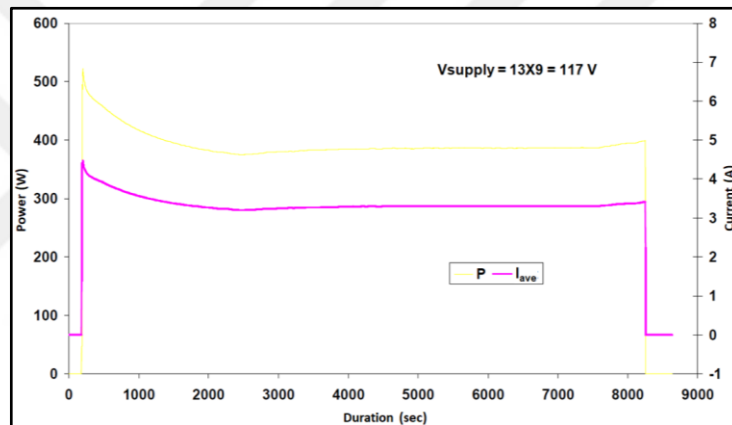
Figure 4.33. Thermoelectric system voltage and current profiles in second prototype

The DC power voltage and current values of the second prototype are shown in Figure 4.33. The thermoelectric modules are powered by three different DC power supplies. Each DC power supply feeds each thermoelectric group where three Peltier modules are serially connected. The voltage of each DC power supply is adjusted to 39 V and thus each module is supplied with 13V. Figure 4.33 shows the transient characteristics of power and current values for thermoelectric modules during the entire drying operation. It should be noted that the profile of the DC current is obtained by keeping the supply voltage to the modules constant. It is apparent from the figure that the maximum DC current takes place at the beginning of the drying operation and the DC current gradually decreases to its steady-state value as the drying operation continues. Therefore, the DC current value is 4.34 A and power value is 510 W in the transient phase while these values decrease to 3.30 A and 385 W in the steady-state drying operation.
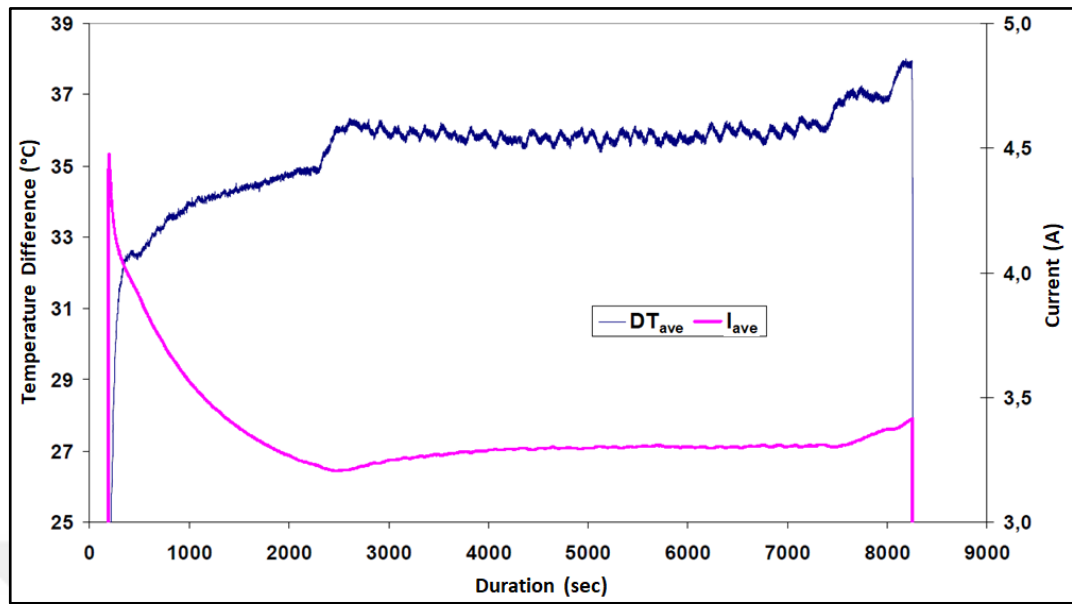
Figure 4.34. Relation between the thermoelectric module temperature difference and the current through the modules

The average surface temperature difference between the hot and cold surfaces of the thermoelectric modules and the DC current through the thermoelectric modules are shown together in Figure 4.34. It is evident that the higher the temperature difference, the lower DC current.
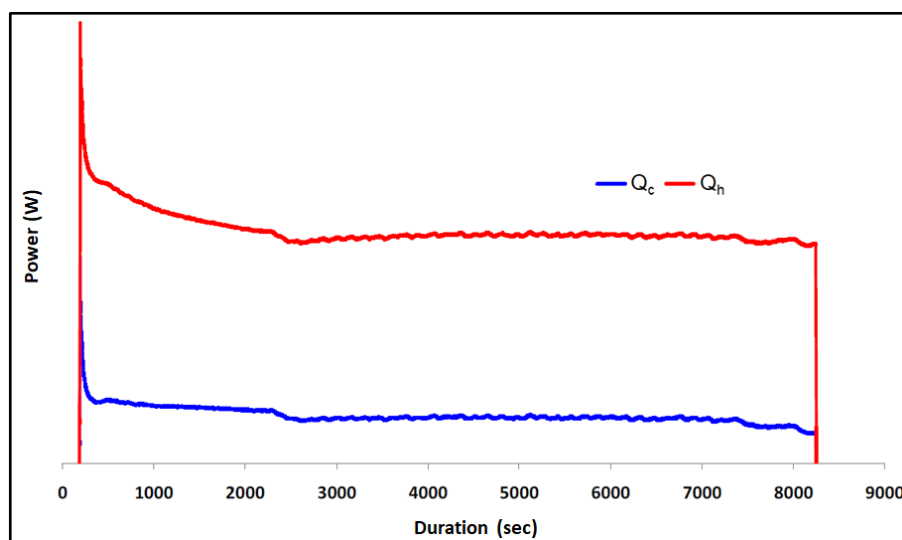
Figure 4.35. Profiles of thermoelectric cooling and heating powers

The profiles of the thermoelectric module cooling and heating powers are presented in Figure 4.35. These values are calculated by making use of the electrical properties which are provided by the thermoelectric module manufacturers. Some of these electrical properties are the maximum feeding voltage (V_{max}), the maximum feeding current (I_{max}) and the maximum temperature difference of module surfaces (DT_{max}). In Table 4.6, the variation of electrical properties for a thermoelectric module is shown at different hot side surface temperatures. Thermoelectric cooling and heating powers are calculated as a function of time using the module surface temperature measured during the drying operation as a function of time.

Table 4.6. Peltier module electrical specifications as a function of hot side temperature

	Material Specifications (27 °C hot side temp.)	Material Specifications (50 °C hot side temp.)
V_{max} (V)	24.60	27.30
I_{max} (A)	7.900	7.900
Q_{max} (W)	120	131.7
DT_{max} (°C)	69	78
Operation Temperature	-40 °C to +200 °C	

Figure 4.35 shows that both the heating power (Q_h) and the cooling power (Q_c) reach their maximum values in the beginning of the operation and start to decrease gradually toward the steady-state phase.
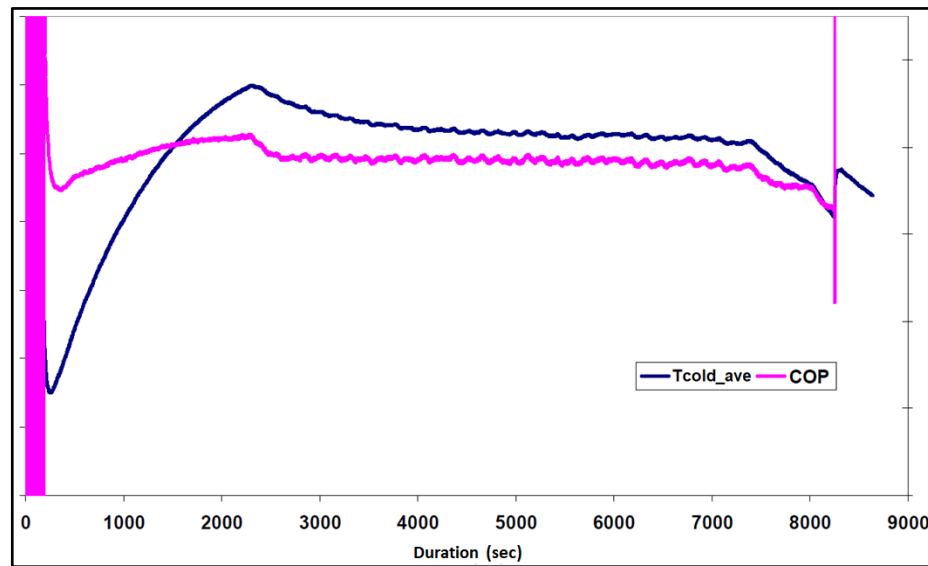
Figure 4.36. The COP profile of second prototype

The COP profile of the thermoelectric module is shown in Figure 4.36. It seems that the COP value is low in the beginning of the operation, increases through the early transient state, reaches its peak value where the cold side temperature is maximum and stabilizes in the course of the transition to steady state. It is noted that the COP value increases with the surface temperature.

The standard energy consumption for the second hybrid dryer prototype is examined out with and without the by-pass feature on the thermoelectric system. The process air flow rate is measured to be 37 l/s without the by-pass channel while 45 l/s with the by-pass. As a result of the experiments, the specific energy consumption value of 0.92 REF* and the water collection efficiency of 74.2 per cent are obtained without the by-pass feature. After the by-pass feature is employed, the specific energy consumption value is slightly reduced to 0.912 REF* while the water collection efficiency is increased to 75.88 per cent.

Table 4.7. Second prototype experiment results without by-pass after 145 minutes

SE wrt REF*	Moist percentage after operation (%)	Water collection efficiency (%)
0.92 REF*	1.930	74.20

Table 4.8. Second prototype experiment results with by-pass after 143 minutes

SE wrt REF*	Moist percentage after operation (%)	Water collection efficiency (%)
0.912 REF*	2.410	75.88
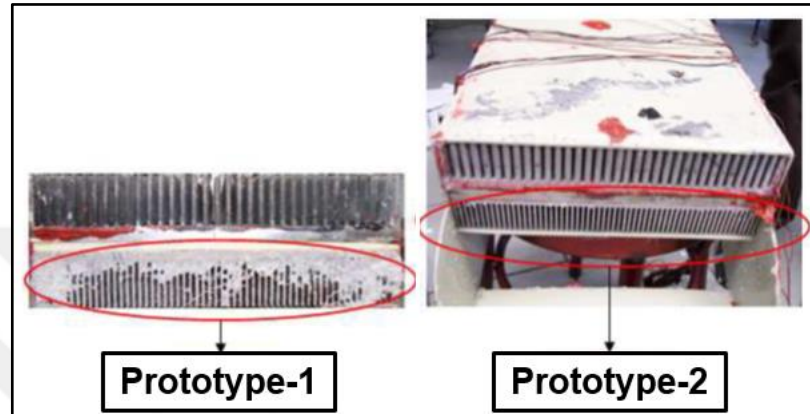
Figure 4.37. Comparison of the tear-down examinations for first and second prototype thermoelectric systems

The tear-down examination is also performed for the second prototype as done in the first prototype to investigate the fiber accumulation at the entrance of the heat exchanger. As shown in Figure 4.37, the improvements on the second prototype considerably reduce the fiber accumulation at the inlet of coldsink compared to the first prototype.

4.3. THE THIRD PROTOTYPE

The focus of the second prototype is structural improvement to resolve several issues observed in the first prototype, and test results shows successful improvement on the machine performance. The third prototype, on the other hand, modifies the thermoelectric system design while preserving the second drying machine prototype. The focus of third prototype is to examine the effect of increased thermoelectric module surfaces. The previous Tetech-120W 40x40 Peltier modules are replaced with larger Tellurex-126W 50x54 Peltier modules whose performance and power specifications are expected to be similar.
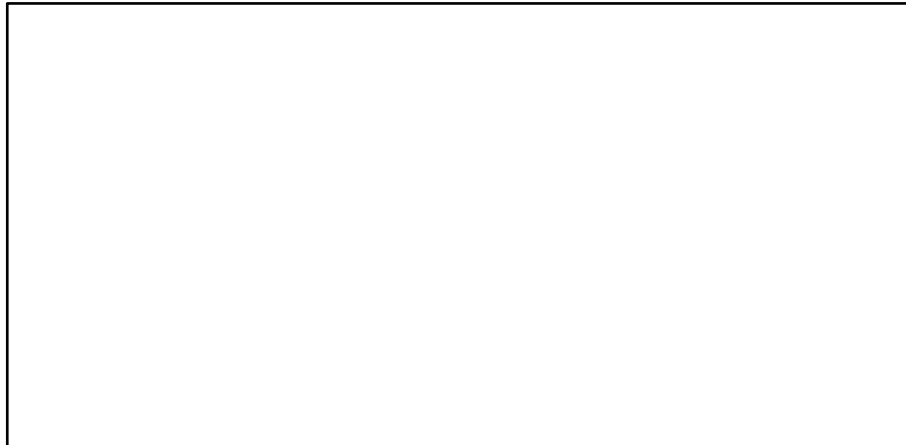
Figure 4.38. Comparison of Tellurex (126W, 50x54) and Tetech (120W, 40x40)

Figure 4.38 shows that the performances of the selected Tellurex and Tetech Peltier modules are very close to each other. Total 12 Tellurex Peltier modules are employed in the third prototype while total nine Peltier modules are used each in the first and second prototype. Consequently, the heatsink bottom surface utilization is increased from 23 per cent to 51 per cent. The twelve thermoelectric modules are divided into 3 groups with 4 modules in each group.
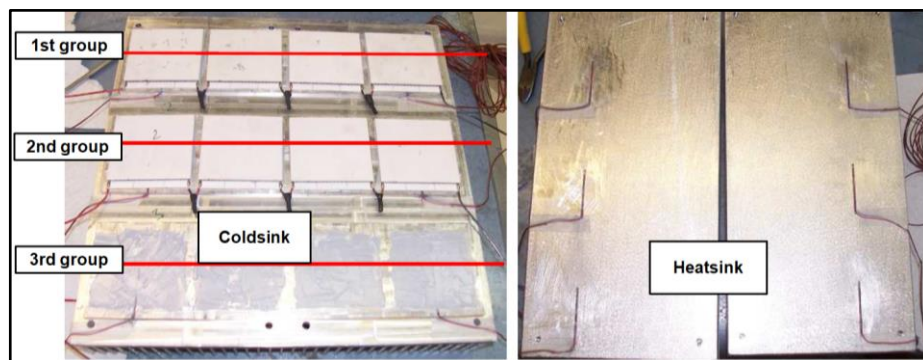
Figure 4.39. Thermoelectric system construction with 12 modules for the third prototype
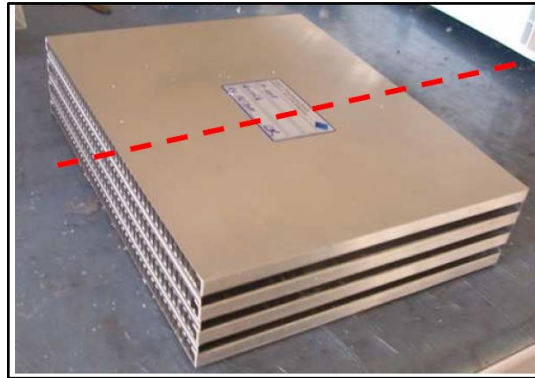
Figure 4.40. Condenser for the third prototype

A brand-new condenser is provided from AKG for the third hybrid dryer prototype. This air-cooled condenser has three channels for the process and 4 channels for the cooling air flow. The dimension of the new condenser is 67 mm in total height, 230 mm in total width and 170 mm in total. The height of each process channel is 7.8 mm while the height of each cooling channel is 9.8 mm. The by-pass feature is implemented to the third prototype during its construction unlike the previous prototypes.
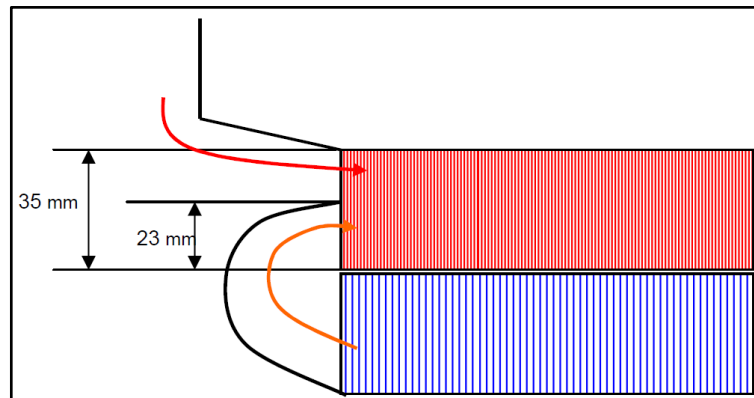
Figure 4.41. Dimensions of the by-pass channel for the third prototype
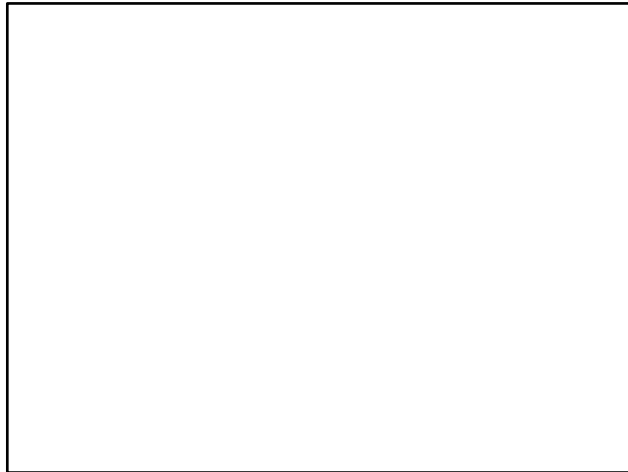
Figure 4.42. Process fan setup capable of frequency adjustment

The process fan is removed from the tumble motor and connected to another motor in order to examine the effect of process air flow rate on the performance. Electric motor revolution can be adjusted by using a frequency inverter on the setup.
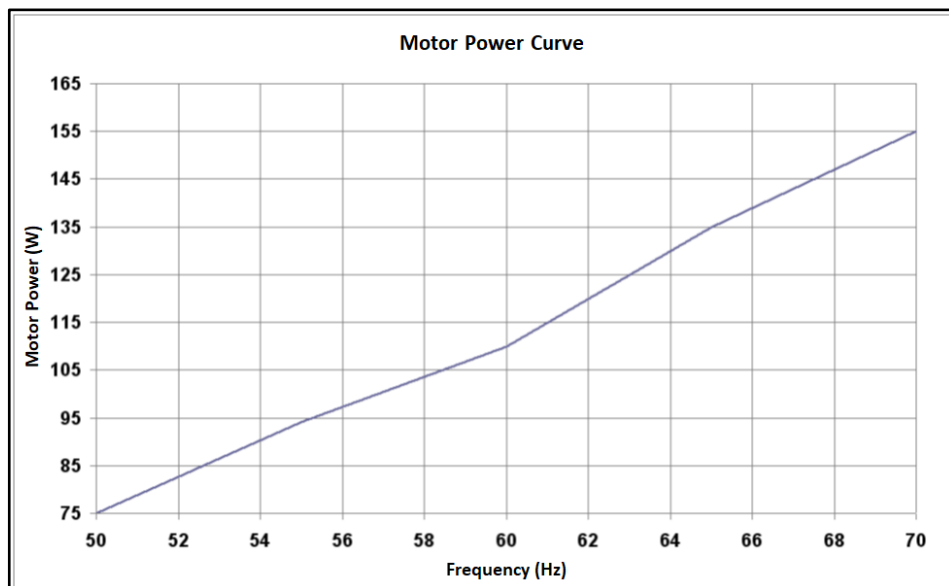
Figure 4.43. Electric motor power curve

4.3.1. The Third Prototype Experiments

The process air flow rates at the third prototype are measured as 41.5 l/s, 48.5 l/s and 52.5 l/s for the motor frequencies of 50 Hz, 60 Hz and 70 Hz, respectively. Standard energy consumption test results with 50 Hz motor frequency are shown in Table 4.9. The specific energy consumption of 0.903 REF* and the water collection efficiency of 80 per cent are obtained during the third prototype 50 Hz tests. Electrical loss is assumed as 15 per cent. The thermoelectric system condensation rate is measured to be 0.11 g/s which renders the power of 260 W withdrawn for condensation.

Table 4.9. Prototype-3 experiment results with 50 Hz

Laundry capacity (kg)	Program duration (min)	Electrical Loss (%)	SE wrt REF*	Moist percentage after operation (%)	Water collection efficiency (%)
8	130	15	0.903 REF*	2.360	80

Standard energy consumption test results with 60 Hz motor frequency are shown in Table 4.10. The specific energy consumption and the water collection efficiency are measured to be 0.897 REF* and 73 per cent, respectively. The increase of the motor power which is related to the frequency adjustment is added to the specific energy consumption.

Table 4.10. Prototype-3 experiment results with 60 Hz

Laundry capacity (kg)	Program duration (min)	Electrical Loss (%)	SE wrt REF*	Moist percentage after operation (%)	Water collection efficiency (%)
8	130	15	0.897 REF*	1.900	73

According to the third prototype experiment results, approximately 1.5 per cent reduction on specific energy consumption is achieved which might be linked to the prototyping variation. It is concluded that the increased surface area of thermoelectric modules has no significant effect on the specific energy consumption.

4.4. THE FOURTH PROTOTYPE

The fourth hybrid dryer prototype attempts to modify the cold side heat exchanger design. The old and new fin geometries of the coldsink are shown in Figure 4.44. Fin thickness and fin gap are increased while the total number of fins is reduced. The fin profile is also changed from rectangular to trapezoidal shape in new coldsink design. Consequently, the pressure drop across the heat exchanger is reduced with these design changes.
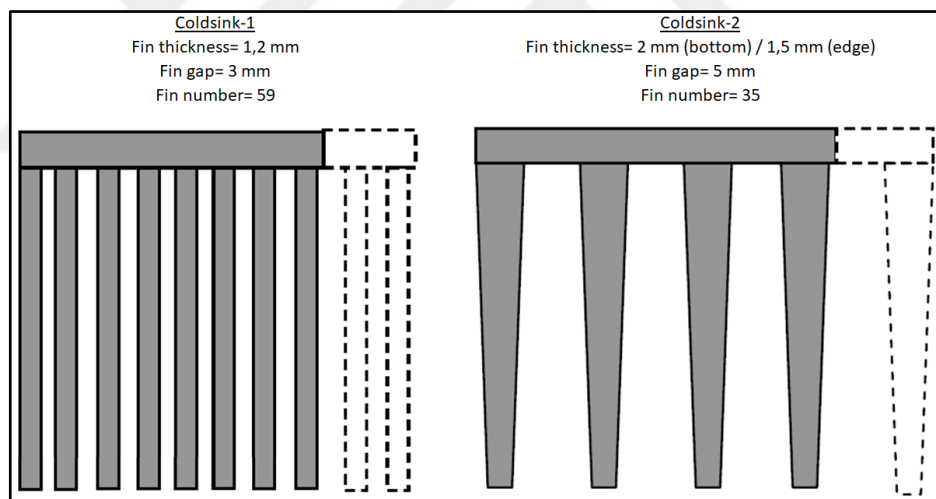
Figure 4.44. Fin geometry comparison of coldsink-1 and coldsink-2

Figure 4.45. Inlet profile comparison of coldsink-1 and coldsink-2

4.4.1. The Fourth Prototype Experiments

The process air flow rates are measured as 46 l/s in 50 Hz motor frequency and 53 l/s in 60 Hz motor frequency on the fourth prototype with by-pass feature.

Standard energy consumption test results with 50 Hz motor frequency are shown in Table 4.11. The specific energy consumption of 0.915 REF* and the water collection efficiency of 78.12 per cent are achieved during the fourth prototype 50 Hz tests. The thermoelectric system condensation rate is measured as 0.125 g/s and the corresponding condensation power is calculated as 290 W.

Table 4.11. Prototype-4 experiment results with 50 Hz

SE wrt REF*	Moist percentage after operation (%)	Water collection efficiency (%)
0.915 REF*	2.530	78.12

Standard energy consumption test results with 60 Hz motor frequency yield the specific energy consumption of 0.875 REF* and the water collection efficiency of 76 per cent as shown in Table 4.12. The thermoelectric system condensation rate is measured to be 0.14 g/s and the corresponding condensation power is calculated as 330 W.

Table 4.12. Prototype-4 experiment results with 60 Hz

SE wrt REF*	Moist percentage after operation (%)	Water collection efficiency (%)
0.875 REF*	1.200	76.00

In the fourth prototype, the coldsink fin surface area is reduced from 0.98 m^2 to 0.6 m^2 by decreasing the number of fins from 59 to 35. As clear in the fourth prototype test results, the increase of motor frequency from 50 Hz to 60 Hz leads to a significant improvement on specific energy consumption. Thermoelectric system condensation rate and energy are also improved.

5. CONCLUSION AND FUTURE WORK

5.1. CONCLUSION

There is a big supply gap in today's tumble dryer market between air condenser tumble dryers which have "B" energy label with lower prices and heat pump tumble dryers which have "A+++" energy label with higher prices. This project has aimed to show that air condenser tumble dryer energy consumption can be improved to the "A" energy label by implementing thermoelectric heat pump modules and that a hybrid tumble dryer can be produced with lower costs than the heat pump tumble dryer.

Firstly, theoretical energy calculations were performed and the target values of significant parameters were determined to be able to achieve the A level of energy consumption by the implementation of thermoelectric modules. Wind tunnel experiments were carried out under specific conditions in order to confirm theoretical calculation results.

Secondly, CFD analyses were conducted with the purpose of gaining a better understanding on the effect of thermoelectric modules arrangement to the heatsink performance. Furthermore, a heatsink testing setup was designed and constructed in order to examine the thermal resistance and pressure drop values of different heatsinks with different air flow rates.

Subsequently, hybrid tumble dryer prototypes were constructed and tested according to the standard energy consumption specification. Several structural problems were noticed in the first prototype. These problems were resolved in the second prototype and further thermoelectric system improvements were conducted in the third and fourth prototypes.

As a result, the specific energy consumption of the reference condenser tumble dryer with "B" label was improved by 12.5 per cent for the best case and it was proven that the hybrid dryer with the thermoelectric heat pump system can achieve A-level of energy consumption.

5.2. FUTURE WORK

The most challenging part of this study was not being able to use the configurations that are patent-protected and developing new configurations. Structural and operational advantages were lost in the beginning of the study. Alternative configurations can be studied in the future to have better condensation rate for energy recovery and better process air flow rate for higher COP.

Analytical modelling of condensation is another roadblock in this study. More experimental data needs to be collected to have condensation rate improvement in the cold side of the thermoelectric system.

Although the heat is needed to be absorbed from the cold surface and conducted through the hot surface of thermoelectric modules as much as possible, this also required the extensive usage of heatsinks made of aluminum. During the drying operation, these aluminum blocks store a significant amount of energy that is not being recovered. Alternative heatsink and coldsink designs with lower mass can be studied without compromising the thermal capacity of the heat exchanger.

In order for the product to be feasible, the cost of components needs to be optimized to have a better price advantage over heat pump tumble dryers. Thus, the number of thermoelectric modules must be optimized with technical and commercial workstreams.

Finally, thermoelectric module COP values are currently lower than other heat pump systems. Any technical achievement or technological breakthrough on thermoelectric systems may provide huge advantage to the patent owners in the future. Therefore, it is important to follow the progress in thermoelectric industry.

REFERENCES

1. Adhikari K. Thermocouple: facts and theories. *Himalayan Physics*. 2017;6:10-14.

2. Harvey R, Walker D, Frampton K. Enhancing performance of thermoelectric coolers through the application of distributed control. *IEEE Transactions on Components and Packaging Technologies*. 2007;30(2):330-336.

3. Bell L. Cooling, heating, generating power, and recovering waste heat with thermoelectric systems. *Science*. 2008;321(5895):1457-1461.

4. Godfrey S. An introduction to thermoelectric coolers | Electronics Cooling. 2018 [Cited 2018 30 March]. Available from: https://www.electronics-cooling.com/1996/09/an-introduction-to-thermoelectric-coolers/.

5. Hájovský R, Pieš M, Richtár L. Analysis of the appropriateness of the use of Peltier cells as energy sources. *Sensors*. 2016;16(6):760-772.

6. Tan F, Fok S. Methodology on sizing and selecting thermoelectric cooler from different TEC manufacturers in cooling system design. *Energy Conversion and Management*. 2008;49(6):1715-1723.

7. Riffat S, Ma X. Optimum selection (design) of thermoelectric modules for large capacity heat pump applications. *International Journal of Energy Research*. 2004;28(14):1231-1242.

8. Riffat S, Ma X. Improving the coefficient of performance of thermoelectric cooling systems: a review. *International Journal of Energy Research*. 2004;28(9):753-768.

9. Stawreberg L. Energy efficiency improvements of tumble dryers. Karlstad: Karlstad University, 2011.

10. Hartoka O. Design of an efficient condenser for tumble dryers. Istanbul: Yeditepe University; 2009.

11. Elshafei E. Effect of flow bypass on the performance of a shrouded longitudinal fin array. *Applied Thermal Engineering*. 2007;27(13):2233-2242.

12. Stawreberg L, Berghel J, Renström R. Energy losses by air leakage in condensing tumble dryers. *Applied Thermal Engineering*. 2012;37:373-379.